

---

# Unifying 2D and 3D Vision-Language Understanding

---

Ayush Jain<sup>\*1,2</sup> Alexander Swerdlow<sup>\*1</sup> Yuzhou Wang<sup>1</sup> Sergio Arnaud<sup>2</sup> Ada Martin<sup>2</sup> Alexander Sax<sup>2</sup>  
Franziska Meier<sup>2</sup> Katerina Fragkiadaki<sup>1</sup>

## Abstract

Progress in 3D vision-language learning has been hindered by the scarcity of large-scale 3D datasets. We introduce UniVLG, a unified architecture for 2D and 3D vision-language understanding that bridges the gap between existing 2D-centric models and the rich 3D sensory data available in embodied systems. Our approach initializes most model weights from pre-trained 2D models and trains on both 2D and 3D vision-language data. We propose a novel language-conditioned mask decoder shared across 2D and 3D modalities to ground objects effectively in both RGB and RGB-D images, outperforming box-based approaches. To further reduce the domain gap between 2D and 3D, we incorporate 2D-to-3D lifting strategies, enabling UniVLG to utilize 2D data to enhance 3D performance. With these innovations, our model achieves state-of-the-art performance across multiple 3D vision-language grounding tasks, demonstrating the potential of transferring advances from 2D vision-language learning to the data-constrained 3D domain. Furthermore, co-training on both 2D and 3D data enhances performance across modalities without sacrificing 2D capabilities. By removing the reliance on 3D mesh reconstruction and ground-truth object proposals, UniVLG sets a new standard for realistic, embodied-aligned evaluation. Code and additional visualizations are available at [univlg.github.io](https://univlg.github.io).

vision-language models to interpret their sensory video input, rather than leveraging 3D models that incorporate depth and egomotion. At first glance, this reliance on 2D models appears counterintuitive, as prior research has consistently shown that 3D models outperform their 2D counterparts when trained on comparable amounts of data (Siddiqui et al., 2023; Kundu et al., 2020a; Fang et al., 2021; Rukhovich et al., 2022). The key limitation, however, is dataset availability: while 2D datasets are vast and well-curated, 3D datasets remain scarce and expensive to annotate (Dai et al., 2017; Yeshwanth et al., 2023). As a result, there are currently no high-performing, pre-trained 3D encoders capable of processing 3D inputs at the same level as CLIP (Radford et al., 2021) does for 2D images. This data imbalance has led to a significant performance gap, ultimately slowing the widespread adoption of 3D models in embodied vision-language systems. Given these challenges, is scaling 3D training data the only viable path to bridging this gap, or are there alternative strategies for making 3D models more effective?

In this paper, we introduce UniVLG, a unified 2D-3D vision-language model designed to improve 3D understanding by leveraging large-scale 2D data and pre-trained 2D models. UniVLG is trained on both 2D and 3D vision-language tasks, including referential grounding, object detection, and question answering in images and 3D scenes. Unlike models that operate directly on 3D point clouds, UniVLG processes RGB and RGB-D images—natural sensory inputs for embodied agents—and supports both single-view RGB images or multi-view posed RGB-D images. UniVLG processes each image with strong pre-trained 2D backbones, which also constitute the majority of its parameters, and fully leverages their representational power. It discriminates between 2D and 3D purely through the positional encodings of 2D image patch features, which represent the 2D pixel grid locations in images and the 3D (X,Y,Z) coordinates in scenes, similar to (Jain et al., 2024). When training on 2D RGB images, we consider both 2D and 3D processing pathways within UniVLG, by using predicted 3D pointmaps (Wang et al., 2024), which further narrows the domain gap between 2D and 3D input. We further introduce a novel language-conditioned mask decoder, shared across both 2D and 3D input, which predicts segmentation masks by conditioning

## 1. Introduction

Today’s real-world embodied systems rely on depth sensors and egocentric, calibrated camera setups for navigation and interaction with their surroundings (Ahn et al., 2022; Chiang et al., 2024). However, despite having access to rich 3D information, these systems predominantly use 2D

<sup>\*</sup>Equal contribution <sup>1</sup>Carnegie Mellon University <sup>2</sup>Meta Inc..  
Correspondence to: Ayush Jain <[ayushj2@andrew.cmu.edu](mailto:ayushj2@andrew.cmu.edu)>, Alexander Swerdlow <[aswerdlow@andrew.cmu.edu](mailto:aswerdlow@andrew.cmu.edu)>.

# Unifying 2D and 3D Vision-Language Understanding

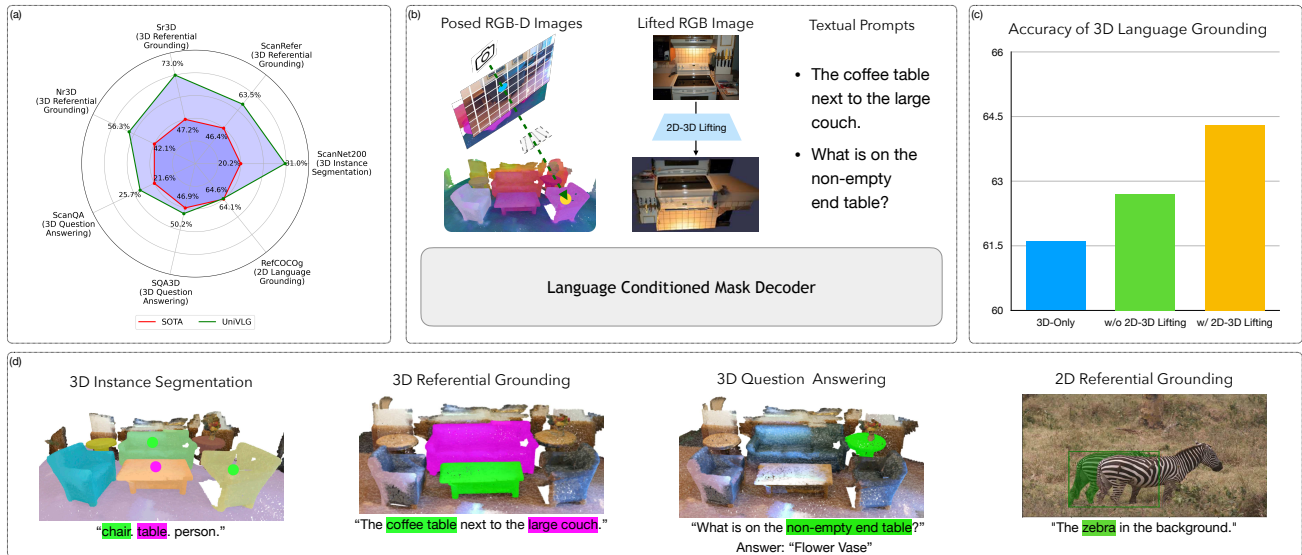


Figure 1. (A) UniVLG achieves state-of-the-art performance across a range of referential grounding, question answering, and instance segmentation benchmarks. (B) UniVLG is a unified model which accepts posed RGB-D sequences, or monocular 2D images which are then lifted to 3D pointmaps. (C) UniVLG significantly benefits from joint 2D-3D training, further boosted when all parameters are shared between modalities by using 2D-3D lifting. (D) Example task inputs/outputs for UniVLG.

on both visual features and language instructions to ground objects mentioned in the language input. Segmentation masks serve as a unifying output representation because they involve per-patch predictions, where each patch corresponds to either a 2D pixel or a 3D point. In our experiments, we show that besides unifying the output space, decoding to 3D masks results in significantly more precise predictions, challenging the established paradigm which decode bounding boxes or rely on object proposals. Our model is designed with the goal of sharing all weights across RGB image and RGB-D image sequence processing.

We test UniVLG on established 2D and 3D vision language benchmarks (Achlioptas et al., 2020; Chen et al., 2020a). We find that when trained exclusively on 3D data, UniVLG achieves state-of-the-art performance across all established benchmarks, outperforming prior methods in comparable settings by more than 15%. Furthermore, co-training UniVLG with 2D data enhances its 3D performance even further, both on in-domain and out-of-domain benchmarks. Notably, this improvement does not come at the expense of 2D tasks—UniVLG retains strong performance on 2D referential grounding datasets (Kazemzadeh et al., 2014) compared to its version which is only trained on 2D referential grounding data. UniVLG directly uses sensor point clouds without any mesh pre-processing of the RGB-D input and without relying on ground-truth bounding box proposals, typically used in existing works and benchmarks (Achlioptas et al., 2020). By benchmarking in these more realistic settings, we hope to encourage future research that aligns more closely with the goals of embodied vision and promotes the progress

of 3D vision in practical, real-world scenarios.

In summary, our contributions are:

- **Unified 2D-3D Visual Grounding:** We propose a model that can consume and benefit from both 2D and 3D vision-language data.
- **State-of-the-Art Performance:** UniVLG achieves state-of-the-art performance on in-domain 3D referential grounding benchmarks, including ReferIt3D (SR3D, NR3D) and ScanRefer, outperforming prior methods by a significant margin, while also excelling in out-of-domain 3D referential grounding datasets.
- **Language-Conditioned 3D Mask Decoder:** We propose a novel language-conditioned mask decoder head for 3D referential grounding and show its superior performance over bounding box decoders.
- **Realistic Evaluation Settings:** We benchmark prior methods and UniVLG in realistic, embodied-aligned settings by using sensor-generated instead of mesh-reconstructed point clouds and without relying on ground-truth object proposals.

We make our code publicly available at [univlg.github.io](https://github.com/univlg).

## 2. Related Work

**Use of 2D data for 3D Visual Language Understanding Tasks** Most 3D Visual Language models directly operate over the provided 3D point clouds without using any 2D pre-trained features. SAT-2D (Yang et al., 2021a) is one

of the first 3D visual grounding model which used 2D visual features during training for aligning 2D and 3D visual features and show significant boost over its versions that do not use 2D features. Recent methods in 3D Question Answering like 3D-LLM (Hong et al., 2023) and NaviLLM (Zheng et al., 2024) use multi-view 2D features and pass them to LLMs for decoding answers. However, so far they haven’t been able to successfully address 3D visual grounding tasks. PQ3D (Zhu et al., 2024b) uses a combination of several visual backbones, including a 2D based feature backbone from OpenScene (Peng et al., 2023b). Recent work of EFM3D (Straub et al., 2024) uses 3D feature volumes obtained from lifting 2D image features but only evaluates on the task of 3D object detection and surface reconstruction.

Another related line of research focuses on enhancing 2D vision-language models (VLMs) with 3D reasoning. Spatial-RGPT (Cheng et al., 2024) and Spatial-VLM (Chen et al., 2024) use depth estimation to enrich 2D models with spatial understanding. While these methods focus on improving 2D perception, our approach leverages 2D-to-3D lifting to enhance multi-view 3D reasoning, bridging the gap between 2D and 3D for vision-language grounding.

The closest work to ours is ODIN (Jain et al., 2024), which also differentiates between 2D and 3D through positional encodings instead of using separate image and point cloud encoders. However, they only consider the task of object segmentation. UniVLG is inspired by ODIN and innovates over it in the following ways: a) It extends its applicability to referential grounding and question-answering tasks. b) It improves the mask decoder to better incorporate language information. c) It shares all parameters between 2D and 3D pathways, instead of a subset of them by lifting 2D images to 3D pointmaps. With these advancements, UniVLG dramatically outperforms ODIN, and its extension LLaVA-3D (Zhu et al., 2024a) on 3D language grounding, demonstrating the importance of its design choices.

**3D Visual Grounding Models** 3D Visual Grounding Models can be broadly divided into two categories: Two-stage methods and single-stage end-to-end methods. Two stage methods first generate 3D object proposals and then select one proposal out of them. This is the dominant paradigm: InstanceRefer (Yuan et al., 2021a), SAT-2D (Yang et al., 2021a), ViL3DRel (Chen et al., 2022) and recently scaled-up to models of 3D-VisTA (Zhu et al., 2023b) and PQ3D (Zhu et al., 2024b) which train their model on multiple 3D datasets and tasks. Specifically, 3D-VisTA first pre-trains their model on masked language/object modeling and scene-text matching, and then fine-tunes to downstream several language understanding tasks of interest. PQ3D (Zhu et al., 2024b) proposes promptable object queries for 3D scene understanding. While it decodes masks for instance segmentation tasks directly, it follows a 2D stage ap-

proach for free-form language grounding and selects a mask from a set of object mask proposals. However, two-stage methods are limited by the failures of the object proposal networks. To overcome this limitation, single-stage methods like 3D-SPS (Luo et al., 2022) and BUTD-DETR (Jain et al., 2022) directly regress 3D bounding boxes. They achieve strong results, especially on benchmarks like ScanRefer, which do not provide ground-truth proposals. However, they have only been trained on individual tasks and datasets and have not been scaled up yet. In this work, we propose a single-stage end-to-end model that is jointly trained on multiple 3D language understanding tasks, and achieve state-of-the-art results on several benchmarks.

For additional related work, see Appendix (Section-A.14).

### 3. Method

We show the architecture of UniVLG in Figure-2. The model takes as input a language query,  $N$  RGB images of shape  $N \times H \times W \times 3$ , and an associated 3D pointmap of shape  $N \times H \times W \times 3$ . The output consists of segmentation masks for each object mentioned in the sentence, a corresponding text span that refers to each segmented object, and optionally, generated text that answers the question. In datasets such as ScanNet, we obtain the 3D pointmap by unprojecting the sensed depth images using the camera parameters and standard pinhole-camera equations. For RGB images from 2D datasets like RefCOCO (Kazemzadeh et al., 2014), we use a neural 2D-to-3D lifting model (Wang et al., 2024), which takes a (monocular) RGB image as input and predicts a 3D pointmap. Note that the 3D pointmap does not need to be metric—in fact, our 3D pointmaps for 2D datasets are represented in relative space.

**Visual Encoder:** We encode each RGB image independently using DiNO ViT encoder (Oquab et al., 2024), and add several 3D attention layers (Jain et al., 2024) on top of features from multiple layers. Specifically, we apply 3D  $k$ -NN attention with relative positional embeddings to fuse information across the input RGB views. This attention mechanism uses feature maps from the ViT encoder, with 3D pointmaps serving as the positional embeddings. Since our attention mechanism is relative, our model does not require a metric pointmap.

**Language Encoder:** We embed the natural language query using JinaCLIP (Koukoumas et al., 2024), generating tokens of shape  $M \times F$  where  $M$  is the number of tokens and  $F$  is the feature dimension.

**Language Conditioned Mask Decoder:** The mask decoder head takes as input the encoded visual features, their corresponding (relative) 3D coordinates, and the encoded language utterance; it outputs 3D segmentation masks of the mentioned objects and a text span over the encoded

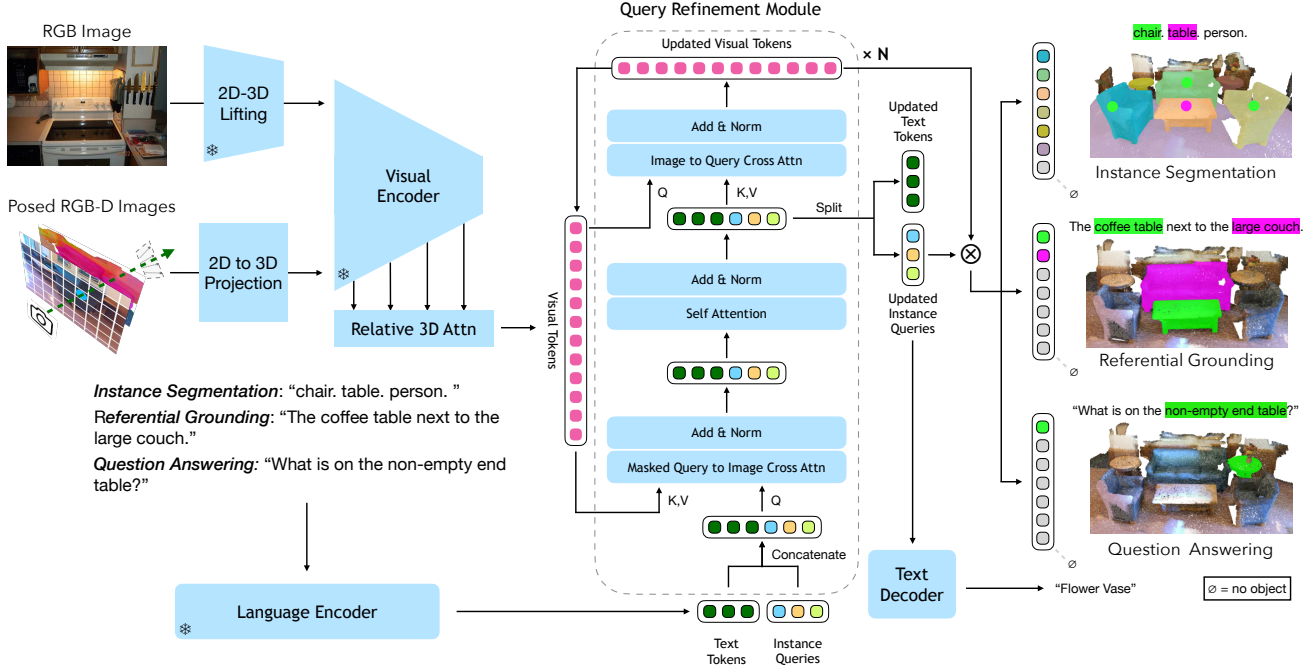


Figure 2. **UniVLG Architecture**: A vision language transformer that accepts a language utterance and either (1) a sequence of posed RGB-D images or (2) a monocular RGB image, lifted to 3D (2D to 3D Projection). UniVLG fuses information across vision and language to predict 3D object segments or generate answers. It uses a ViT backbone followed by 3D relative attentions to produce a set of 3D feature tokens. The proposed decoder then iteratively updates a set of learnable queries as well as the 3D feature tokens through token - language - query attentions to decode object segments and match them to noun phrases in the input referential utterance. Masks are decoded through a dot-product between 3D feature tokens and learnable queries. A text decoder predicts answers for the input questions by conditioning on the set of updated object queries.

language utterance. Our mask decoder head draws inspiration from Mask2Former (Cheng et al., 2022) and makes important architectural changes to make it suitable for 3D referential grounding.

We initialize a set of  $M$  learnable object queries, each responsible for decoding an object instance. We concatenate these object queries with the language tokens along the sequence dimension. We alternate between cross-attention between these and the visual tokens and self-attention among these concatenated queries and text tokens. Instead of using a vanilla cross-attention layer, we follow Mask2Former and use a masked variant where each query only attends to the points falling within the corresponding instance mask predicted by the previous layer. For this operation, we add 3D positional embeddings on the visual features. Next, the visual tokens from the backbone are updated by cross-attending to the updated object and text tokens. Specifically, let  $Q^{(0)} \in \mathbb{R}^{M \times D}$  be the initial object queries,  $T \in \mathbb{R}^{L \times D}$  be the text tokens, and  $V^{(0)} \in \mathbb{R}^{N \times D}$  be the 3D visual tokens. The query refinement process can be described as:

$$\begin{aligned} X^{(0)} &= [Q^{(0)}; T]; \\ X^{(i+1)} &= \text{Norm}(\text{MaskedCrossAttention}(X^{(i)}, V^{(i)}) + X^{(i)}) \\ X^{(i+1)} &= \text{Norm}(\text{SelfAttention}(X^{(i+1)}) + X^{(i+1)}) \\ V^{(i+1)} &= \text{Norm}(\text{CrossAttention}(V^{(i)}, X^{(i+1)}) + V^{(i)}), \end{aligned}$$

where  $[\cdot]$  denotes concatenation along the sequence dimension, and  $i$  is the layer index. The refined queries after each decoder layer  $Q^{(i+1)} = X_{1:M}^{(i+1)}$  are then used for mask prediction with the updated visual features and for language grounding.

We find that *updating visual features* via attention to queries and text tokens is crucial for 3D-referential grounding. Open-vocabulary mask decoders, such as those in ODIN (Jain et al., 2024) and X-Decoder (Zou et al., 2023), which extend Mask2Former’s decoder to accept language tokens, do not update visual features during query refinement as in our method. Although their approach is sufficient for 3D instance segmentation, our experiments show that this choice significantly hinders performance in decoding object masks for 3D referential grounding (Table 7). Object2Scene (Zhu et al., 2023a), which decodes 3D bounding boxes for referential grounding, finds that only updating



queries is sufficient. However, our ablation studies show that while this holds true for bounding box decoding, updating visual features during query refinement is crucial for accurately decoding masks (Table 5b).

After attending to text and visual features, the refined object queries decode object segments through a token-wise dot-product with the updated visual features to produce mask logits which are then thresholded to obtain segmentation masks:

$$M_i = \sigma(\text{sigmoid}(Q_i^{(f)} \cdot V^T)), \quad (1)$$

where  $M_i$  is the mask for the  $i$ -th object query,  $\sigma$  is a threshold function, and  $\cdot$  denotes dot product.

**Text Decoder:** Beyond decoding segments, the refined object queries are used as input to the decoder of a pre-trained T5 (Raffel et al., 2020) decoder to generate answers to questions, following PQ3D (Zhu et al., 2024b). This is useful for question-answering tasks where the output is a text sentence.

### 3.1. Supervision Objective

**Mask Loss:** We match queries to ground-truth instances using Hungarian Matching (Carion et al., 2020). We supervise the matched queries’s predicted masks with both a Binary Cross Entropy (BCE) and Dice loss following Mask2Former (Cheng et al., 2022).

**Text Span Loss:** Similar to prior works (Li et al., 2022; Kamath et al., 2021; Jain et al., 2022), we match the predicted 3D object segmentations to the relevant noun phrases in the input utterance through a dot-product between the object queries and the language tokens, generating the distribution  $G_i$  over the input text sentence for the  $i$ th query:

$$G_i = \text{sigmoid}(f_\phi(Q_i^{(f)}) \cdot f_\theta(T^T)) \quad (2)$$

where  $f_\phi$  and  $f_\theta$  are MLPs,  $G_i$  is the grounding distribution for the  $i$ -th object query over the input text tokens. We supervise these grounding distributions with a BCE loss, with unmatched queries supervised to have a low probability.

**Box Loss:** We observe a failure mode in our model where, when trained with the aforementioned objectives, some masks include a small number of distant, unrelated points, or multiple instances of the same object category are predicted by a single object query (see Figure 5 in Appendix). To address this, we introduce a novel box loss. This loss computes an enclosing 3D bounding box for each predicted mask and supervises it using standard box prediction losses—L1 and Generalized Intersection-over-Union (GIoU) (Rezatofighi et al., 2019)—against the ground-truth bounding boxes. We incorporate this box loss as an additional cost in both Hungarian matching and the final loss. This encourages the model to produce more accurate and compact masks, leading to improved downstream performance.

**Text Generation Loss:** For question answering tasks, our model decodes a text utterance as an output. We supervise

the generated text with the ground-truth text answer using standard cross-entropy loss. In summary, our complete loss function is as follows:

$$\mathcal{L}_{\text{total}} = \lambda_{\text{mask}}\mathcal{L}_{\text{mask}} + \lambda_{\text{text}}\mathcal{L}_{\text{text}} + \lambda_{\text{box}}\mathcal{L}_{\text{box}} + \lambda_{\text{gen}}\mathcal{L}_{\text{gen}} \quad (3)$$

where  $\mathcal{L}_{\text{mask}}$  is the mask loss comprised of binary cross entropy and dice losses,  $\mathcal{L}_{\text{text}}$  is the loss for matching the object queries to the mentioned objects in the language sentence,  $\mathcal{L}_{\text{box}}$  are the additional bounding box losses described earlier, and  $\mathcal{L}_{\text{gen}}$  is the cross-entropy loss over the auto-regressively generated answer (in case of question-answering datasets).

UniVLG shares all learnable parameters between 2D and 3D by leveraging 2D-to-3D lifting strategies to generate pointmaps for 2D datasets, which are seamlessly integrated into 3D attention layers. Additionally, the mask decoding head unifies the output space between 2D and 3D as per-pixel segmentation masks, enabling the sharing of both loss functions and decoder parameters across modalities.

**Implementation details:** UniVLG consists of 108M trainable parameters along with a frozen 220M parameter text-encoder (Koukounas et al., 2024) and a 304M parameter image-encoder (Oquab et al., 2024). At test time, we feed all images to our model with a 90-frame scene taking  $\sim 1050$ ms and  $\sim 15$ GB of VRAM on an A100 GPU. We refer to Appendix A.2 for further details.

## 4. Experiments

We evaluate our model on 3D and 2D referential grounding, 3D question answering and 3D instance segmentation benchmarks. We train our model on the 3D referential grounding datasets of SR3D, NR3D (Achlioptas et al., 2020) and ScanRefer (Chen et al., 2020a) and 3D instance segmentation datasets of ScanNet200 (Rozenberszki et al., 2022) and Matterport3D (Chang et al., 2017). In addition to the 3D datasets, we also train our model on 2D referential grounding datasets with RefCOCO, RefCOCO+ and RefCOCOg (Kazemzadeh et al., 2014), and 2D image segmentation dataset with COCO (Lin et al., 2014). We present results for two model versions: one trained solely on 3D data (UniVLG-3D-only) and the other trained jointly on both 2D and 3D datasets (UniVLG).

### 4.1. Evaluation on 3D Referential Grounding

Following BUTD-DETR (Jain et al., 2022), we test on two evaluation setups: 1. `Det`, where our model and baselines do not have access to ground-truth 3D boxes of objects in the scene, and 2. `GT`, where our model and baselines use ground-truth 3D object proposals provided in the benchmarks.

Additionally, these benchmarks sample point clouds from reconstructed and post-processed meshes instead of directly using the raw point clouds obtained from sensor inputs. As observed in prior works (Jain et al., 2024; Kundu

Table 1. Results on 3D language grounding in 3D mesh and sensor point clouds (PC). We evaluate top-1 accuracy on the official validation set with assuming ground-truth (GT) or without assuming ground-truth proposals (Det).

| Method                                 | SR3D                |                     |                     | Acc<br>(GT) | NR3D                |                     |                     | Acc<br>(GT) | ScanRefer           |                     |                     |
|--|---------------------|---------------------|---------------------|-------------|---------------------|---------------------|---------------------|-------------|---------------------|---------------------|---------------------|
|  | Acc<br>@25<br>(Det) | Acc<br>@50<br>(Det) | Acc<br>@75<br>(Det) |             | Acc<br>@25<br>(Det) | Acc<br>@50<br>(Det) | Acc<br>@75<br>(Det) |             | Acc<br>@25<br>(Det) | Acc<br>@50<br>(Det) | Acc<br>@75<br>(Det) |
| ReferIt3DNet (Achlioptas et al., 2020) | 27.7                | -                   | -                   | 39.8        | 24.0                | -                   | -                   | -           | 26.4                | 16.9                | -                   |
| ScanRefer (Chen et al., 2020a)         | -                   | -                   | -                   | -           | -                   | -                   | -                   | -           | 35.5                | 22.4                | -                   |
| InstanceRefer (Yuan et al., 2021b)     | 31.5                | -                   | -                   | 48.0        | 29.9                | -                   | -                   | -           | 40.2                | 32.9                | -                   |
| LanguageRefer (Roh et al., 2022)       | 39.5                | -                   | -                   | 56.0        | 28.6                | -                   | -                   | -           | -                   | -                   | -                   |
| Mesh SAT-2D (Yang et al., 2021b)       | 35.4                | -                   | -                   | 57.9        | 31.7                | -                   | -                   | -           | 44.5                | 30.1                | -                   |
| PC BUTD-DETR (Jain et al., 2022)       | 52.1                | -                   | -                   | 67.0        | 43.3                | -                   | -                   | 54.6        | 52.2                | 39.8                | -                   |
| 3D-VisTA (Zhu et al., 2023b)           | 56.5                | 51.5                | 42.8                | 76.4        | 47.7                | 42.2                | 35.5                | 65.1        | 51.0                | 46.2                | 36.7                |
| LLaVA-3D (Zhu et al., 2024a)           | -                   | -                   | -                   | -           | -                   | -                   | -                   | -           | 54.1                | 42.2                | -                   |
| PQ3D (Zhu et al., 2024b)               | <b>62.0</b>         | <b>55.9</b>         | <b>46.2</b>         | <b>79.7</b> | <b>52.2</b>         | <b>45.0</b>         | <b>37.6</b>         | <b>66.7</b> | <b>56.7</b>         | <b>51.8</b>         | <b>43.3</b>         |
| Sensor ODIN (Jain et al., 2024)        | 38.1                | 29.3                | 23.1                | -           | 31.6                | 20.8                | 15.8                | -           | 43.1                | 33.4                | 26.2                |
| PC BUTD-DETR (Jain et al., 2022)       | 43.3                | 28.9                | 6.58                | -           | 32.2                | 19.4                | 3.64                | -           | 42.2                | 27.9                | 6.53                |
| 3D-VisTA (Zhu et al., 2023b)           | 47.2                | 43.2                | 36.1                | 61.4        | 42.1                | 37.4                | 32.0                | 54.2        | 46.4                | 42.5                | 36.3                |
| UniVLG-3D-only (Ours)                  | 71.6                | 63.8                | 49.4                | <b>78.9</b> | 52.5                | 43.3                | 34.2                | <b>65.8</b> | 60.7                | 53.2                | 42.6                |
| UniVLG (Ours)                          | <b>73.0</b>         | <b>64.8</b>         | <b>51.8</b>         | -           | <b>56.3</b>         | <b>48.0</b>         | <b>37.6</b>         | -           | <b>63.5</b>         | <b>56.4</b>         | <b>46.0</b>         |

et al., 2020a), mesh-sampled point clouds often exhibit fine-grained misalignment with sensor-generated point clouds, which can unfairly disadvantage sensor-based approaches on these benchmarks. To address this, we benchmark our method and prior methods in a more embodied-aligned setting using sensor point clouds directly. We thus evaluate all methods on benchmark-provided point clouds sampled from the post-processed mesh (*Mesh*), and separately retrain and evaluate a subset of methods on sensor point clouds (*Sensor*) obtained by unprojecting posed RGB-D images.

**Evaluation Metrics:** We use the standard top-1 accuracy metric. For the `Det` setup, a predicted bounding box is considered correct if its intersection over union (IoU) with the ground truth box is higher than a predetermined threshold (we use the standard 0.25, 0.5 and 0.75). As UniVLG predicts masks (instead of axis-aligned bounding boxes), we obtain a bounding box by taking the extents of the mask. For the `GT` setup, we pool visual features inside the given ground-truth masks, and the object queries predict a segmentation mask over the “pooled” feature tokens, one token per object. The prediction is correct if the model selects the feature token corresponding to the ground-truth object.

**Baselines:** We compare our model against the state-of-the-art two-stage methods of 3D-VisTA (Zhu et al., 2023b), PQ3D (Zhu et al., 2024b) and concurrent work of LLaVA-3D (Zhu et al., 2024a); and the SOTA single-stage method of BUTD-DETR (Jain et al., 2022). UniVLG uses significantly less 3D training data than prior SOTA 3D referential grounding models. For example, 3D-VisTA (Zhu et al., 2023b) trains on the previously mentioned 3D datasets that we use but also includes 3RScan (1500 scenes) (Wald et al., 2019), Objaverse (700k objects) (Deitke et al., 2022), and additional text sentences on ScanNet generated using GPT-3 (see Table-3 of 3D-VisTA). Similarly, PQ3D adds the

Multi3DRefer (Zhang et al., 2023) and Scan2Cap datasets (Chen et al., 2020b), but also utilizes a point encoder that was trained on all 3D-VisTA datasets. All two-stage baselines assume access to ground-truth proposals at test-time in the SR3D and NR3D benchmarks; hence we re-evaluate them with predicted boxes coming from a SoTA object detector, Mask3D (Schult et al., 2023). We also re-train 3D-VisTA and BUTD-DETR with sensor point clouds. Despite our best efforts, we could not manage to re-train PQ3D with sensor point clouds due to their use of multiple backbones, and multi-stage training strategies. We also compare our model with ODIN (Jain et al., 2024) trained for 3D language grounding using their architecture but our grounding losses. The 3D referential grounding results are presented in Table 1, from which we find:

**UniVLG outperforms prior methods, regardless of data selection, on all setups which do not assume GT boxes.**

Even without our joint 2D training strategy—and with less 3D data than prior methods—UniVLG-3D-only significantly outperforms all prior methods. It dramatically outperforms alternative single stage models, such as BUTD-DETR, on the stricter IoU threshold of 0.75, thanks to predicting masks instead of bounding boxes—as we demonstrate later in Table 5c. In the `GT` setup as well, UniVLG significantly outperforms 3D-VisTA and closely matches the performance of the recent work of PQ3D in the setup where PQ3D uses mesh point clouds, while UniVLG operates over sensor point clouds.

**Co-training UniVLG with 2D and 3D data enhances 3D performance** across all 3D vision-language grounding benchmarks, demonstrating that leveraging 2D data during training provides additional benefits beyond initializing the model with pre-trained 2D weights (row-5, sensor PC, Table 8).

Table 2. **Out-of-Domain 3D Referential Grounding** Acc@25 in Det. From left-to-right, ScanNet++, HM3D, ARKitScenes, ScanNet (GT), ScanNet (SAMPro3D). See Appendix A.3 for details.

| Model          | SN++        | HM3D        | ARKit       | SN-GT       | SN-SAM      |
|----------------|-------------|-------------|-------------|-------------|-------------|
| UniVLG-3D-only | 42.4        | 49.7        | 64.6        | 77.0        | 50.9        |
| UniVLG         | <b>42.8</b> | <b>51.9</b> | <b>65.1</b> | <b>79.9</b> | <b>52.5</b> |

Table 3. **Results on 3D Visual Question Answering** on official validation sets. We evaluate top-1 exact match accuracy (EM@1).

|           | Method                                    | ScanQA      | SQA3D       |
|-----------|---|-------------|-------------|
| Mesh PC   | 3D-LLM (BLIP2-flant5) (Hong et al., 2023) | 20.5        | -           |
|           | PQ3D (Zhu et al., 2024b)                  | 21.0        | 47.0        |
|           | 3D-VisTA (Zhu et al., 2023b)              | 22.1        | <b>47.5</b> |
|           | NaviLLM (Zheng et al., 2024)              | <b>23.9</b> | -           |
| Sensor PC | 3D-VisTA (Zhu et al., 2023b)              | 21.6        | 46.9        |
|           | UniVLG (Ours)                             | <b>25.7</b> | <b>50.2</b> |

### Performance of all prior SOTA models drop with sensor point cloud as input and without assuming GT boxes:

Both single-stage methods like BUTD-DETR and two-stage methods like 3D-VisTA have a performance drop of 5-15% when using sensor RGB-D point clouds as input instead of mesh point-clouds. The sensor point cloud and mesh point clouds have fine-grained misalignment, resulting in this drop. Shifting from ground-truth box proposals to a more realistic setup of using predicted box proposals from a SOTA detector results in a drop of 15-20% in accuracy. Nonetheless, even when UniVLG uses sensor pointclouds (which as we showed above result in a 5-15% accuracy drop on these benchmarks), it still outperforms the baselines that use *mesh* point clouds as input.

Qualitative results of UniVLG are in Figure 3 (Appendix).

## 4.2. Evaluation on Out-of-Domain 3D Referential Grounding

We evaluate our model and baselines on LX3D<sup>†</sup>, an out-of-domain 3D language grounding dataset that spans ScanNet (Dai et al., 2017), ScanNet++ (Yeshwanth et al., 2023), ARKitScenes (Baruch et al., 2021), and HM3D (Yadav et al., 2023) (details in Appendix A.3). LX3D allows us to assess the robustness of our model on new scenes, camera capture systems, and language instructions. We show the results of our model, both a 3D-only variant and our full model w/2D data + lifting in Table 2. We find that our model outperforms prior methods on these out-of-domain datasets, achieving strong performance across the board.

## 4.3. Evaluation on 3D Question Answering

We test UniVLG on ScanQA (Azuma et al., 2022) and SQA3D (Ma et al., 2022) question answering benchmarks. ScanQA (Azuma et al., 2022) focuses on spatial relations. Alongside question-answer pairs, the dataset includes an-

<sup>†</sup>LX3D is contributed by a concurrent anonymous submission and is not part of our contributions.

Table 4. **Results on val sets of 2D Ref. grounding datasets**

|                                  | RefCOCO | RefCOCO+ | RefCOCOg |
|----------------------------------|---------|----------|----------|
| LAVT (Yang et al., 2022) (B)     | 72.7    | 62.4     | 61.2     |
| ReSTR (Kim et al., 2022)         | 67.2    | 55.7     | 54.5     |
| X-Decoder (T) (Zou et al., 2023) | -       | -        | 61.9     |
| X-Decoder (B) (Zou et al., 2023) | -       | -        | 64.5     |
| X-Decoder (L) (Zou et al., 2023) | -       | -        | 64.6     |
| UniVLG (2D only)                 | 69.4    | 61.3     | 64.0     |
| UniVLG (2D-3D)                   | 69.2    | 61.3     | 64.1     |

notations for the objects referenced in the question, and we supervise our model to predict these in addition to generating the answer. SQA3D (Ma et al., 2022) provides pairs of situation descriptions and questions regarding embodied scene understanding, navigation, common sense and multi-hop reasoning, such as, “*looking for some food in the fridge*”, “*which direction should i go?*” and the task is to generate the correct answer (“*right*”).

**Evaluation Metrics:** We use the established Exact Match (EM@1) metric, which measures if the generated answer matches either of the two answer candidates provided by ScanQA, or the single ground-truth answer provided by SQA3D. We also report results with additional metrics in Appendix (Table 11).

**Baselines:** We compare against the LLM based methods of 3D-LLM (Hong et al., 2023) and NaviLLM (Zheng et al., 2024) which use BLIP2-flanT5 (Li et al., 2023) and Vicuna-7B (Peng et al., 2023a) as their answer generation heads. We also compare with 3D-VisTA (Zhu et al., 2023b) and PQ3D (Zhu et al., 2024b) which use small decoder heads like T5-small (Raffel et al., 2020), similar to our approach. We show results in Table 3 on the validation sets of these benchmarks. UniVLG outperforms all prior baselines on both benchmarks. We found that using sensor point clouds vs mesh point clouds does not result in a significant difference in performance in these benchmarks, likely because the models are evaluated on text generation instead of localization of objects as in 3D referential grounding and segmentation benchmarks.

Additionally, we show results on 3D instance segmentation in Appendix A.1.

## 4.4. Evaluation on 2D Referential Grounding

We also evaluate UniVLG on the 2D Referential Grounding benchmarks (Kazemzadeh et al., 2014) (Table 4). We train two versions of our model: UniVLG (2D only), which is trained exclusively on 2D datasets, and UniVLG (2D-3D), which is trained on both 2D and 3D data. Our results show that co-training with 3D data does not degrade the performance of the version trained solely on 2D data. This demonstrates that it is indeed possible to train a single model for both 2D and 3D tasks. As we show in our experiments, this approach leads to significant improvements in 3D performance without negatively affecting 2D performance. In this

Table 5. Analysis of Box Head vs Mask Head on ScanRefer Dataset with Acc@25 if not otherwise stated.

| (a) Parametric vs Non-parametric Query |             |             | (b) Updating Visual Features |             |             | (c) Results at Various IoU Thresholds |             |             |
|--|-------------|-------------|------------------------------|-------------|-------------|---------------------------------------|-------------|-------------|
| Query Type                             | Box Head    | Mask Head   | Feat Attn                    | Box Head    | Mask Head   | Acc@25                                | Acc@75      |             |
| Param                                  | 23.9        | <b>54.4</b> | ✓                            | 33.9        | <b>54.4</b> | Box Head                              | 34.5        | 1.1         |
| Non-param                              | <b>34.5</b> | 43.9        | ✗                            | <b>34.5</b> | 41.5        | Mask Head                             | <b>54.4</b> | <b>33.2</b> |

Table 6. Analysis of 2D training strategies Acc@25 in DetSetup

| Model                           | Avg Accuracy | SR3D        | NR3D        | ScanRefer   |
|---------------------------------|--------------|-------------|-------------|-------------|
| UniVLG-3D-only                  | 61.6         | 71.6        | 52.5        | 60.7        |
| UniVLG-2D-3D(w/o 2D-3D lifting) | 62.7         | 73.0        | 53.5        | 61.5        |
| UniVLG-2D-3D(w/ 2D-3D lifting)  | <b>64.3</b>  | <b>73.0</b> | <b>56.3</b> | <b>63.5</b> |

Table 7. Ablations Acc@25 in DetSetup

| Model                           | Avg Accuracy | SR3D        | NR3D        | ScanRefer   |
|---------------------------------|--------------|-------------|-------------|-------------|
| UniVLG                          | <b>61.0</b>  | <b>67.1</b> | <b>55.7</b> | <b>60.2</b> |
| w/o mask decoder w/ box decoder | 39.3         | 38.9        | 33.2        | 45.7        |
| w/o feature attn                | 36.9         | 38.0        | 30.0        | 42.8        |
| w/o pretrained 2D weights       | 53.4         | 54.3        | 49.1        | 56.9        |
| w/o mask bounding box loss      | 56.8         | 64.3        | 49.5        | 56.7        |

work, due to our focus on improving 3D vision-language grounding and resource constraints, we did not train our model on additional 2D datasets, which is common in prior work. Scaling up these models with more 2D data and studying its impact on 3D vision-language grounding is a promising avenue for future research.

#### 4.5. Ablations

We ablate a series of design choices of our model on referential grounding datasets of SR3D, NR3D, and ScanRefer on Table 6 and Table 7; and on ScanRefer dataset in Table 5. We have the following conclusions:

##### 1. Lifting 2D datasets to 3D improves 3D performance.

In Table 6, we compare three variants of our model: one trained only on 3D data, one trained with 3D data and 2D images without lifting them to 3D (where the 3D layers are skipped for 2D inputs, following (Jain et al., 2024)), and our proposed approach of lifting 2D images to 3D pointmaps. We observe that incorporating 2D data improves performance in both scenarios, but our approach of lifting 2D images to 3D achieves the best results. In Appendix A.11, we show in a more controlled setting that training without using 3D pointmaps—by skipping the 3D layers—results in significant overfitting to individual 2D-3D domains.

##### 2. Decoding boxes is inferior to decoding segmentations.

Shifting from decoding segmentation masks to decoding bounding boxes hurts performance (row 2 of Table 7), especially in tight IoU thresholds IoU@0.75, shown in Table 5c.

##### 3. Visual tokens updating through attending to language and queries during mask decoding is essential for good

performance in 3D referential grounding, as shown in row 3 of Table 7. This is potentially because the mask decoding head relies on dot-products of queries and features to predict masks; and thus having both object queries and visual features to be very well distinguished for different instances of the same object is crucial. This design choice is unique to mask decoding heads, as we show in Table 5b. Box-decoding models work similarly well irrespective of updating the visual tokens with language and object tokens. This variant is very close to ODIN’s open vocabulary head, which also lacks such attention operations, and as we show it does not work well for referential language grounding.

##### 4. 2D feature pretraining dramatically improves performance as shown in row 4 of Table 7.

##### 5. The predicted mask bounding box loss helps significantly as shown in row 5 of Table 7.

##### 6. Non-Parametric Queries are crucial for decoding boxes prediction, while parametric queries work well for decoding segments.

There are two popular choices for object queries: *Parametric Queries* which are scene-independent learnable vectors, initialized from scratch, and are updated via attention. *Non-Parametric Queries*, which are scene-dependent, and are typically initialized by doing Farthest Point Sampling on the input point clouds and encoding the corresponding xyz locations as query positional embeddings and corresponding features as query feature embeddings. Using non-parametric queries are crucial for box-decoding heads, while both queries work similarly well for mask-decoding heads (Table 5a). Box-decoding heads need to regress raw XYZ coordinates in 3D space; the search space is large and sparse—as most of it is empty—and parametric queries have difficulty handling such free space, as already mentioned in 3DETR (Misra et al., 2021). Mask decoding uses dot-product between queries and visual tokens coming from the 3D backbone, and thus does not need to reason about 3D free space.

## 5. Conclusion

We present UniVLG, a vision-language model that integrates 2D and 3D data to address data scarcity in 3D vision-language learning. By leveraging pre-trained 2D features, 2D-to-3D lifting strategies, and a novel mask decoder head, UniVLG significantly outperforms prior methods in realistic embodied 3D vision settings while maintaining strong 2D



understanding. Our extensive ablations validate key design choices: (1) Mask decoding is superior to box decoding, and each proposed component is crucial for its success. (2) Pre-trained 2D features improve performance, and co-training 3D vision-language tasks with 2D data provides additional gains. (3) Incorporating 2D-to-3D lifting strategies further enhances 3D understanding when training with 2D data. More broadly, our findings suggest that scaling 3D data is not the only path forward—leveraging 2D data and pre-trained features can effectively enhance 3D reasoning. We hope UniVLG inspires further research into vision-language models that bridge 2D and 3D for real-world applications.

## Impact Statement

Our work aims to advance 3D vision-language learning by leveraging pre-trained 2D models and 2D-to-3D lifting strategies to overcome the data scarcity in 3D datasets. This approach has the potential to make 3D vision more accessible and practical, particularly for embodied AI applications such as robotics, assistive technologies, and augmented reality. By reducing reliance on large-scale 3D annotations, our method could democratize research in 3D vision and lower computational and data collection costs.

However, as with any vision-language model, there are ethical considerations, including biases inherited from pre-trained 2D models, potential misuse in surveillance applications, and the environmental impact of large-scale model training. We encourage future work to explore methods for mitigating biases in pre-trained models and improving the transparency and interpretability of 3D vision-language systems.

Overall, we believe our contributions will positively impact the field of 3D vision-language learning, enabling progress toward more robust and generalizable embodied AI systems while being mindful of ethical considerations.

## 6. Acknowledgements

The authors express gratitude to Nikolaos Gkanatsios, Wen-Hsuan Chu, Gabriel Sarch, Mathew Bronars, and Naitik Khandelwal for their valuable feedback on the early draft of this work. Special thanks to Kyle Genova for several insightful discussions during the early stages of this project’s development. The authors also thank Cortex team at Meta for valuable feedback and discussions.

## References

Abdelreheem, A., Olszewski, K., Lee, H.-Y., Wonka, P., and Achlioptas, P. Scanents3d: Exploiting phrase-to-3d-object correspondences for improved visio-linguistic models in 3d scenes, 2023. URL <https://arxiv.org/abs/2212.06250>.

[org/abs/2212.06250](https://arxiv.org/abs/2212.06250).

Achlioptas, P., Abdelreheem, A., Xia, F., Elhoseiny, M., and Guibas, L. ReferIt3D: Neural Listeners for Fine-Grained 3D Object Identification in Real-World Scenes. In *Proc. ECCV*, 2020.

Ahn, M., Brohan, A., Brown, N., Chebotar, Y., Cortes, O., David, B., Finn, C., Fu, C., Gopalakrishnan, K., Hausman, K., Herzog, A., Ho, D., Hsu, J., Ibarz, J., Ichter, B., Irpan, A., Jang, E., Ruano, R. J., Jeffrey, K., Jesmonth, S., Joshi, N. J., Julian, R., Kalashnikov, D., Kuang, Y., Lee, K.-H., Levine, S., Lu, Y., Luu, L., Parada, C., Pastor, P., Quiambao, J., Rao, K., Rettinghouse, J., Reyes, D., Sermanet, P., Sievers, N., Tan, C., Toshev, A., Vanhoucke, V., Xia, F., Xiao, T., Xu, P., Xu, S., Yan, M., and Zeng, A. Do as i can, not as i say: Grounding language in robotic affordances, 2022. URL <https://arxiv.org/abs/2204.01691>.

Azuma, D., Miyanishi, T., Kurita, S., and Kawanabe, M. Scanqa: 3d question answering for spatial scene understanding. In *proceedings of the IEEE/CVF conference on computer vision and pattern recognition*, pp. 19129–19139, 2022.

Baruch, G., Chen, Z., Dehghan, A., Dimry, T., Feigin, Y., Fu, P., Gebauer, T., Joffe, B., Kurz, D., Schwartz, A., et al. Arkitscenes: A diverse real-world dataset for 3d indoor scene understanding using mobile rgb-d data. *arXiv preprint arXiv:2111.08897*, 2021.

Carion, N., Massa, F., Synnaeve, G., Usunier, N., Kirillov, A., and Zagoruyko, S. End-to-End Object Detection with Transformers. In *Proc. ECCV*, 2020.

Chang, A., Dai, A., Funkhouser, T., Halber, M., Niessner, M., Savva, M., Song, S., Zeng, A., and Zhang, Y. Matterport3d: Learning from rgb-d data in indoor environments. *arXiv preprint arXiv:1709.06158*, 2017.

Chen, B., Xu, Z., Kirmani, S., Ichter, B., Driess, D., Florence, P., Sadigh, D., Guibas, L., and Xia, F. Spatialvlm: Endowing vision-language models with spatial reasoning capabilities, 2024. URL <https://arxiv.org/abs/2401.12168>.

Chen, D. Z., Chang, A., and Nießner, M. ScanRefer: 3D Object Localization in RGB-D Scans using Natural Language. In *Proc. ECCV*, 2020a.

Chen, D. Z., Gholami, A., Nießner, M., and Chang, A. X. Scan2cap: Context-aware dense captioning in rgb-d scans, 2020b.

Chen, S., Guhur, P.-L., Tapaswi, M., Schmid, C., and Laptev, I. Language conditioned spatial relation reasoning for 3d object grounding. *Advances in neural information processing systems*, 35:20522–20535, 2022.

- Cheng, A.-C., Yin, H., Fu, Y., Guo, Q., Yang, R., Kautz, J., Wang, X., and Liu, S. Spatialrgpt: Grounded spatial reasoning in vision language models, 2024. URL <https://arxiv.org/abs/2406.01584>.
- Cheng, B., Misra, I., Schwing, A. G., Kirillov, A., and Girdhar, R. Masked-attention mask transformer for universal image segmentation. 2022.
- Chiang, H.-T. L., Xu, Z., Fu, Z., Jacob, M. G., Zhang, T., Lee, T.-W. E., Yu, W., Schenck, C., Rendleman, D., Shah, D., Xia, F., Hsu, J., Hoech, J., Florence, P., Kirmani, S., Singh, S., Sindhvani, V., Parada, C., Finn, C., Xu, P., Levine, S., and Tan, J. Mobility vla: Multimodal instruction navigation with long-context vlms and topological graphs, 2024. URL <https://arxiv.org/abs/2407.07775>.
- Chibane, J., Engelmann, F., Anh Tran, T., and Pons-Moll, G. Box2mask: Weakly supervised 3d semantic instance segmentation using bounding boxes. In *European conference on computer vision*, pp. 681–699. Springer, 2022.
- Dai, A., Chang, A. X., Savva, M., Halber, M., Funkhouser, T., and Nießner, M. Scannet: Richly-annotated 3d reconstructions of indoor scenes. In *Proceedings of the IEEE conference on computer vision and pattern recognition*, pp. 5828–5839, 2017.
- Deitke, M., Schwenk, D., Salvador, J., Weihs, L., Michel, O., VanderBilt, E., Schmidt, L., Ehsani, K., Kembhavi, A., and Farhadi, A. Objaverse: A universe of annotated 3d objects. *arXiv preprint arXiv:2212.08051*, 2022.
- Dubey, A., Jauhri, A., Pandey, A., Kadian, A., Al-Dahle, A., Letman, A., Mathur, A., Schelten, A., Yang, A., Fan, A., Goyal, A., Hartshorn, A. S., Yang, A., Mitra, A., Srivankumar, A., Korenev, A., Hinsvark, A., Rao, A., Zhang, A., Rodriguez, A., Gregerson, A., Spataru, A., tiste Roziere, B., Biron, B., Tang, B., Chern, B., Caucheteux, C., Nayak, C., Bi, C., Marra, C., McConnell, C., Keller, C., Touret, C., Wu, C., Wong, C., Ferrer, C. C., Nikolaidis, C., Allonsius, D., Song, D., Pintz, D., Livshits, D., Esiobu, D., Choudhary, D., Mahajan, D., Garcia-Olano, D., Perino, D., Hupkes, D., Lakomkin, E., AlBadawy, E. A., Lobanova, E., Dinan, E., Smith, E. M., Radenovic, F., Zhang, F., Synnaeve, G., Lee, G., Anderson, G. L., Nail, G., Mialon, G., Pang, G., Cucurell, G., Nguyen, H., Korevaar, H., Xu, H., Touvron, H., Zarov, I., Ibarra, I. A., Kloumann, I. M., Misra, I., Evtimov, I., Copet, J., Lee, J., Geffert, J. L., Vranes, J., Park, J., Mahadeokar, J., Shah, J., van der Linde, J., Billock, J., Hong, J., Lee, J., Fu, J., Chi, J., Huang, J., Liu, J., Wang, J., Yu, J., Bitton, J., Spisak, J., Park, J., Rocca, J., Johnstun, J., Saxe, J., Jia, J.-Q., Alwala, K. V., Upasani, K., Plawiak, K., Li, K., neth Heafield, K.-., Stone, K., El-Arini, K., Iyer, K., Malik, K., ley Chiu, K., Bhalla, K., Rantala-Yeary, L., van der Maaten, L., Chen, L., Tan, L., Jenkins, L., Martin, L., Madaan, L., Malo, L., Blecher, L., Landzaat, L., de Oliveira, L., Muzzi, M., Pasupuleti, M. B., Singh, M., Paluri, M., Kardas, M., Oldham, M., Rita, M., Pavlova, M., Kambadur, M. H. M., Lewis, M., Si, M., Singh, M. K., Hassan, M., Goyal, N., Torabi, N., Bashlykov, N., Bogoychev, N., Chatterji, N. S., Duchenne, O., cCelebi, O., Alrassy, P., Zhang, P., Li, P., Vasić, P., Weng, P., Bhargava, P., Dubal, P., Krishnan, P., Koura, P. S., Xu, P., He, Q., Dong, Q., Srinivasan, R., Ganapathy, R., Calderer, R., Cabral, R. S., Stojnic, R., Raileanu, R., Girdhar, R., Patel, R., main Sauvestre, R., Polidoro, R., Sumbaly, R., Taylor, R., Silva, R., Hou, R., Wang, R., Hosseini, S., Chennabasappa, S., Singh, S., Bell, S., Kim, S. S., Edunov, S., Nie, S., Narang, S., Raparthy, S. C., Shen, S., Wan, S., Bhosale, S., Zhang, S., Vandenhende, S., Batra, S., Whitman, S., Sootla, S., Collot, S., Gururangan, S., Borodinsky, S., Herman, T., Fowler, T., Sheasha, T., Georgiou, T., Scialom, T., Speckbacher, T., Mihaylov, T., Xiao, T., Karn, U., Goswami, V., Gupta, V., Ramanathan, V., Kerkez, V., Gonguet, V., Do, V., Vogeti, V., Petrovic, V., Chu, W., Xiong, W., Fu, W., ney Meers, W., Martinet, X., Wang, X., Tan, X. E., Xie, X., Jia, X., Wang, X., Goldschlag, Y., Gaur, Y., Babaei, Y., Wen, Y., Song, Y., Zhang, Y., Li, Y., Mao, Y., Coudert, Z. D., Yan, Z., Chen, Z., Papakipos, Z., Singh, A. K., Grattafiori, A., Jain, A., Kelsey, A., Shajnfeld, A., Gangidi, A., Victoria, A., Goldstand, A., Menon, A., Sharma, A., Boesenberg, A., Vaughan, A., Baeviski, A., Feinstein, A., Kallet, A., Sangani, A., Yunus, A., Lupu, A., Alvarado, A., Caples, A., Gu, A., Ho, A., Poulton, A., Ryan, A., Ramchandani, A., Franco, A., Saraf, A., Chowdhury, A., Gabriel, A., Bharambe, A., Eisenman, A., Yazdan, A., James, B., Maurer, B., Leonhardi, B., Huang, P.-Y. B., Loyd, B., Paola, B. D., Paranjape, B., Liu, B., Wu, B., Ni, B., Hancock, B., Wasti, B., Spence, B., Stojkovic, B., Gamido, B., Montalvo, B., Parker, C., Burton, C., Mejia, C., Wang, C., Kim, C., Zhou, C., Hu, C., Chu, C.-H., Cai, C., Tindal, C., Feichtenhofer, C., Civin, D., Beaty, D., Kreymer, D., Li, S.-W., Wyatt, D., Adkins, D., Xu, D., Testuggine, D., David, D., Parikh, D., Liskovich, D., Foss, D., Wang, D., Le, D., Holland, D., Dowling, E., Jamil, E., Montgomery, E., Presani, E., Hahn, E., Wood, E., Brinkman, E., Arcaute, E., Dunbar, E., Smothers, E., Sun, F., Kreuk, F., Tian, F., Ozgenel, F., Caggioni, F., Guzm'an, F., Kanayet, F. J., Seide, F., Florez, G. M., Schwarz, G., Badeer, G., Swee, G., Halpern, G., Thattai, G., Herman, G., Sizov, G. G., Zhang, G., Lakshminarayanan, G., Shojanazeri, H., Zou, H., Wang, H., Zha, H., Habeeb, H., Rudolph, H., Suk, H., Aspegren, H., Goldman, H., Molybog, I., Tufanov, I., Veliche, I.-E., Gat, I., Weissman, J., Geboski, J., Kohli, J., Asher, J., Gaya, J.-B., Marcus, J., Tang, J., Chan, J., Zhen, J., Reizenstein, J., Teboul, J., Zhong, J.,

- Jin, J., Yang, J., Cummings, J., Carvill, J., Shepard, J., McPhie, J., Torres, J., Ginsburg, J., Wang, J., Wu, K., KamHou, U., Saxena, K., Prasad, K., Khandelwal, K., Zand, K., Matosich, K., Veeraraghavan, K., Michelena, K., Li, K., Huang, K., Chawla, K., Lakhota, K., Huang, K., Chen, L., Garg, L., Lavender, A., Silva, L., Bell, L., Zhang, L., Guo, L., Yu, L., Moshkovich, L., Wehrstedt, L., Khabsa, M., Avalani, M., Bhatt, M., Tsimpoukelli, M., Mankus, M., Hasson, M., Lennie, M., Reso, M., Groshev, M., Naumov, M., Lathi, M., Keneally, M., Seltzer, M. L., Valko, M., Restrepo, M., Patel, M., Vyatskov, M., Samvelyan, M., Clark, M., Macey, M., Wang, M., Hermoso, M. J., Metanat, M., Rastegari, M., Bansal, M., Santhanam, N., Parks, N., White, N., Bawa, N., Singhal, N., Egebo, N., Usunier, N., Laptev, N. P., Dong, N., Zhang, N., Cheng, N., Chernoguz, O., Hart, O., Salpekar, O., Kalinli, O., Kent, P., Parekh, P., Saab, P., Balaji, P., Rittner, P., Bontrager, P., Roux, P., Dollár, P., Zvyagina, P., Ratanchandani, P., Yuvraj, P., Liang, Q., Alao, R., Rodriguez, R., Ayub, R., Murthy, R., Nayani, R., Mitra, R., Li, R., Hogan, R., Battey, R., Wang, R., Maheswari, R., Howes, R., Rinott, R., Bondu, S. J., Datta, S., Chugh, S., Hunt, S., Dhillon, S., Sidorov, S., Pan, S., Verma, S., Yamamoto, S., Ramaswamy, S., Lindsay, S., Feng, S., Lin, S., Zha, S. C., Shankar, S., Zhang, S., Wang, S., Agarwal, S., Sajuyigbe, S., Chintala, S., Max, S., Chen, S., Kehoe, S., Satterfield, S., Govindaprasad, S., Gupta, S., Cho, S.-B., Virk, S., Subramanian, S., Choudhury, S., Goldman, S., Remez, T., Glaser, T., Best, T., Kohler, T., Robinson, T., Li, T., Zhang, T., Matthews, T., Chou, T., Shaked, T., Vontimitta, V., Ajayi, V., Montanez, V., Mohan, V., Kumar, V. S., Mangla, V., Ionescu, V., Poenaru, V. A., Mihailescu, V. T., Ivanov, V., Li, W., Wang, W., Jiang, W., Bouaziz, W., Constable, W., Tang, X., Wang, X., Wu, X., Wang, X., Xia, X., Wu, X., Gao, X., Chen, Y., Hu, Y., Jia, Y., Qi, Y., Li, Y., Zhang, Y., Zhang, Y., Adi, Y., Nam, Y., Wang, Y., Hao, Y., Qian, Y., He, Y., Rait, Z., DeVito, Z., Rosnbrick, Z., Wen, Z., Yang, Z., and Zhao, Z. The llama 3 herd of models. *ArXiv*, abs/2407.21783, 2024. URL <https://api.semanticscholar.org/CorpusID:271571434>.
- Fang, Z., Jain, A., Sarch, G., Harley, A. W., and Fragkiadaki, K. Move to see better: Self-improving embodied object detection, 2021. URL <https://arxiv.org/abs/2012.00057>.
- Hong, Y., Zhen, H., Chen, P., Zheng, S., Du, Y., Chen, Z., and Gan, C. 3d-llm: Injecting the 3d world into large language models. *Advances in Neural Information Processing Systems*, 36:20482–20494, 2023.
- Hu, E. J., Shen, Y., Wallis, P., Allen-Zhu, Z., Li, Y., Wang, S., Wang, L., and Chen, W. Lora: Low-rank adaptation of large language models. *arXiv preprint arXiv:2106.09685*, 2021.
- Jain, A., Gkanatsios, N., Mediratta, I., and Fragkiadaki, K. Bottom up top down detection transformers for language grounding in images and point clouds. In *European Conference on Computer Vision*, pp. 417–433. Springer, 2022.
- Jain, A., Katara, P., Gkanatsios, N., Harley, A. W., Sarch, G., Aggarwal, K., Chaudhary, V., and Fragkiadaki, K. Odin: A single model for 2d and 3d segmentation. In *Proceedings of the IEEE/CVF Conference on Computer Vision and Pattern Recognition*, pp. 3564–3574, 2024.
- Kamath, A., Singh, M., LeCun, Y. A., Misra, I., Synnaeve, G., and Carion, N. MDETR - Modulated Detection for End-to-End Multi-Modal Understanding. In *Proc. ICCV*, 2021.
- Kazemzadeh, S., Ordonez, V., Matten, M., and Berg, T. ReferItGame: Referring to objects in photographs of natural scenes. In Moschitti, A., Pang, B., and Daelemans, W. (eds.), *Proceedings of the 2014 Conference on Empirical Methods in Natural Language Processing (EMNLP)*, pp. 787–798, Doha, Qatar, October 2014. Association for Computational Linguistics. doi: 10.3115/v1/D14-1086. URL <https://aclanthology.org/D14-1086/>.
- Kim, N., Kim, D., Lan, C., Zeng, W., and Kwak, S. Restr: Convolution-free referring image segmentation using transformers, 2022. URL <https://arxiv.org/abs/2203.16768>.
- Kirillov, A., Mintun, E., Ravi, N., Mao, H., Rolland, C., Gustafson, L., Xiao, T., Whitehead, S., Berg, A. C., Lo, W.-Y., et al. Segment anything. *arXiv preprint arXiv:2304.02643*, 2023.
- Kolve, E., Mottaghi, R., Han, W., VanderBilt, E., Weihs, L., Herrasti, A., Deitke, M., Ehsani, K., Gordon, D., Zhu, Y., et al. Ai2-thor: An interactive 3d environment for visual ai. *arXiv preprint arXiv:1712.05474*, 2017.
- Koukouonas, A., Mastrapas, G., Günther, M., Wang, B., Martens, S., Mohr, I., Sturua, S., Akram, M. K., Martínez, J. F., Ognawala, S., et al. Jina clip: Your clip model is also your text retriever. *arXiv preprint arXiv:2405.20204*, 2024.
- Kundu, A., Yin, X., Fathi, A., Ross, D., Brewington, B., Funkhouser, T., and Pantofaru, C. Virtual multi-view fusion for 3d semantic segmentation, 2020a. URL <https://arxiv.org/abs/2007.13138>.

- Kundu, A., Yin, X., Fathi, A., Ross, D., Brewington, B., Funkhouser, T., and Pantofaru, C. Virtual multi-view fusion for 3d semantic segmentation. In *Computer Vision–ECCV 2020: 16th European Conference, Glasgow, UK, August 23–28, 2020, Proceedings, Part XXIV 16*, pp. 518–535. Springer, 2020b.
- Lai, X., Yuan, Y., Chu, R., Chen, Y., Hu, H., and Jia, J. Mask-attention-free transformer for 3d instance segmentation. In *Proceedings of the IEEE/CVF International Conference on Computer Vision*, pp. 3693–3703, 2023.
- Li, J., Li, D., Savarese, S., and Hoi, S. Blip-2: Bootstrapping language-image pre-training with frozen image encoders and large language models. In *International conference on machine learning*, pp. 19730–19742. PMLR, 2023.
- Li, L. H., Zhang, P., Zhang, H., Yang, J., Li, C., Zhong, Y., Wang, L., Yuan, L., Zhang, L., Hwang, J.-N., et al. Grounded language-image pre-training. In *Proceedings of the IEEE/CVF Conference on Computer Vision and Pattern Recognition*, pp. 10965–10975, 2022.
- Lin, T.-Y., Maire, M., Belongie, S., Hays, J., Perona, P., Ramanan, D., Dollár, P., and Zitnick, C. L. Microsoft coco: Common objects in context. In *Computer Vision–ECCV 2014: 13th European Conference, Zurich, Switzerland, September 6–12, 2014, Proceedings, Part V 13*, pp. 740–755. Springer, 2014.
- Liu, Z., Lin, Y., Cao, Y., Hu, H., Wei, Y., Zhang, Z., Lin, S., and Guo, B. Swin transformer: Hierarchical vision transformer using shifted windows. In *Proceedings of the IEEE/CVF international conference on computer vision*, pp. 10012–10022, 2021.
- Lu, J., Deng, J., Wang, C., He, J., and Zhang, T. Query refinement transformer for 3d instance segmentation. In *Proceedings of the IEEE/CVF International Conference on Computer Vision*, pp. 18516–18526, 2023.
- Luo, J., Fu, J., Kong, X., Gao, C., Ren, H., Shen, H., Xia, H., and Liu, S. 3d-sps: Single-stage 3d visual grounding via referred point progressive selection. In *Proceedings of the IEEE/CVF Conference on Computer Vision and Pattern Recognition*, pp. 16454–16463, 2022.
- Ma, X., Yong, S., Zheng, Z., Li, Q., Liang, Y., Zhu, S.-C., and Huang, S. Sqa3d: Situated question answering in 3d scenes. *arXiv preprint arXiv:2210.07474*, 2022.
- Misra, I., Girdhar, R., and Joulin, A. An end-to-end transformer model for 3d object detection. In *Proceedings of the IEEE/CVF international conference on computer vision*, pp. 2906–2917, 2021.
- Oquab, M., Darcet, T., Moutakanni, T., Vo, H., Szafraniec, M., Khalidov, V., Fernandez, P., Haziza, D., Massa, F., El-Nouby, A., Assran, M., Ballas, N., Galuba, W., Howes, R., Huang, P.-Y., Li, S.-W., Misra, I., Rabbat, M., Sharma, V., Synnaeve, G., Xu, H., Jegou, H., Mairal, J., Labatut, P., Joulin, A., and Bojanowski, P. Dinov2: Learning robust visual features without supervision, 2024. URL <https://arxiv.org/abs/2304.07193>.
- Peng, B., Li, C., He, P., Galley, M., and Gao, J. Instruction tuning with gpt-4. *arXiv preprint arXiv:2304.03277*, 2023a.
- Peng, S., Genova, K., Jiang, C., Tagliasacchi, A., Pollefeys, M., Funkhouser, T., et al. Openscene: 3d scene understanding with open vocabularies. In *Proceedings of the IEEE/CVF Conference on Computer Vision and Pattern Recognition*, pp. 815–824, 2023b.
- Radford, A., Kim, J. W., Hallacy, C., Ramesh, A., Goh, G., Agarwal, S., Sastry, G., Askell, A., Mishkin, P., Clark, J., et al. Learning transferable visual models from natural language supervision. In *International conference on machine learning*, pp. 8748–8763. PMLR, 2021.
- Raffel, C., Shazeer, N., Roberts, A., Lee, K., Narang, S., Matena, M., Zhou, Y., Li, W., and Liu, P. J. Exploring the limits of transfer learning with a unified text-to-text transformer. *Journal of machine learning research*, 21 (140):1–67, 2020.
- Rezatofighi, H., Tsoi, N., Gwak, J., Sadeghian, A., Reid, I., and Savarese, S. Generalized intersection over union: A metric and a loss for bounding box regression. In *Proceedings of the IEEE/CVF conference on computer vision and pattern recognition*, pp. 658–666, 2019.
- Robert, D., Vallet, B., and Landrieu, L. Learning multi-view aggregation in the wild for large-scale 3d semantic segmentation. In *Proceedings of the IEEE/CVF Conference on Computer Vision and Pattern Recognition*, pp. 5575–5584, 2022.
- Roh, J., Desingh, K., Farhadi, A., and Fox, D. Language-refer: Spatial-language model for 3d visual grounding. In *Conference on Robot Learning*, pp. 1046–1056. PMLR, 2022.
- Rozenberszki, D., Litany, O., and Dai, A. Language-grounded indoor 3d semantic segmentation in the wild. In *European Conference on Computer Vision*, pp. 125–141. Springer, 2022.
- Rukhovich, D., Vorontsova, A., and Konushin, A. Imvoxelnet: Image to voxels projection for monocular and multi-view general-purpose 3d object detection. In *Proceedings of the IEEE/CVF Winter Conference on Applications of Computer Vision*, pp. 2397–2406, 2022.



- Schult, J., Engelmann, F., Hermans, A., Litany, O., Tang, S., and Leibe, B. Mask3d: Mask transformer for 3d semantic instance segmentation. In *2023 IEEE International Conference on Robotics and Automation (ICRA)*, pp. 8216–8223. IEEE, 2023.
- Siddiqui, Y., Porzi, L., Bulò, S. R., Müller, N., Nießner, M., Dai, A., and Kotschieder, P. Panoptic lifting for 3d scene understanding with neural fields. In *Proceedings of the IEEE/CVF Conference on Computer Vision and Pattern Recognition*, pp. 9043–9052, 2023.
- Straub, J., DeTone, D., Shen, T., Yang, N., Sweeney, C., and Newcombe, R. Efm3d: A benchmark for measuring progress towards 3d egocentric foundation models, 2024. URL <https://arxiv.org/abs/2406.10224>.
- Sturm, J., Engelhard, N., Endres, F., Burgard, W., and Cremers, D. A benchmark for the evaluation of rgb-d slam systems. In *2012 IEEE/RSJ International Conference on Intelligent Robots and Systems*, pp. 573–580, 2012. doi: 10.1109/IROS.2012.6385773.
- Wald, J., Avetisyan, A., Navab, N., Tombari, F., and Nießner, M. Rio: 3d object instance re-localization in changing indoor environments. In *Proceedings of the IEEE/CVF International Conference on Computer Vision*, pp. 7658–7667, 2019.
- Wang, R., Xu, S., Dai, C., Xiang, J., Deng, Y., Tong, X., and Yang, J. Moge: Unlocking accurate monocular geometry estimation for open-domain images with optimal training supervision. *arXiv preprint arXiv:2410.19115*, 2024.
- Wang, T., Mao, X., Zhu, C., Xu, R., Lyu, R., Li, P., Chen, X., Zhang, W., Chen, K., Xue, T., Liu, X., Lu, C., Lin, D., and Pang, J. Embodiedscan: A holistic multi-modal 3d perception suite towards embodied ai, 2023. URL <https://arxiv.org/abs/2312.16170>.
- Xu, M., Yin, X., Qiu, L., Liu, Y., Tong, X., and Han, X. Sampro3d: Locating sam prompts in 3d for zero-shot scene segmentation, 2023. URL <https://arxiv.org/abs/2311.17707>.
- Yadav, K., Ramrakhya, R., Ramkrishnan, S. K., Gervet, T., Turner, J., Gokaslan, A., Maestre, N., Chang, A. X., Batra, D., Savva, M., et al. Habitat-matterport 3d semantics dataset. In *Proceedings of the IEEE/CVF Conference on Computer Vision and Pattern Recognition*, pp. 4927–4936, 2023.
- Yang, Z., Zhang, S., Wang, L., and Luo, J. SAT: 2D Semantics Assisted Training for 3D Visual Grounding. In *Proc. ICCV*, 2021a.
- Yang, Z., Zhang, S., Wang, L., and Luo, J. Sat: 2d semantics assisted training for 3d visual grounding. In *Proceedings of the IEEE/CVF International Conference on Computer Vision*, pp. 1856–1866, 2021b.
- Yang, Z., Wang, J., Tang, Y., Chen, K., Zhao, H., and Torr, P. H. S. Lavt: Language-aware vision transformer for referring image segmentation, 2022. URL <https://arxiv.org/abs/2112.02244>.
- Yeshwanth, C., Liu, Y.-C., Nießner, M., and Dai, A. Scan-net++: A high-fidelity dataset of 3d indoor scenes. In *Proceedings of the IEEE/CVF International Conference on Computer Vision*, pp. 12–22, 2023.
- Yuan, Z., Yan, X., Liao, Y., Zhang, R., Li, Z., and Cui, S. InstanceRefer: Cooperative Holistic Understanding for Visual Grounding on Point Clouds through Instance Multi-level Contextual Referring. In *Proc. ICCV*, 2021a.
- Yuan, Z., Yan, X., Liao, Y., Zhang, R., Wang, S., Li, Z., and Cui, S. Instancerefer: Cooperative holistic understanding for visual grounding on point clouds through instance multi-level contextual referring. In *Proceedings of the IEEE/CVF International Conference on Computer Vision*, pp. 1791–1800, 2021b.
- Zhang, Y., Gong, Z., and Chang, A. X. Multi3drefer: Grounding text description to multiple 3d objects. In *Proceedings of the IEEE/CVF International Conference on Computer Vision*, pp. 15225–15236, 2023.
- Zheng, D., Huang, S., Zhao, L., Zhong, Y., and Wang, L. Towards learning a generalist model for embodied navigation. In *Proceedings of the IEEE/CVF Conference on Computer Vision and Pattern Recognition*, pp. 13624–13634, 2024.
- Zhu, C., Zhang, W., Wang, T., Liu, X., and Chen, K. Object2scene: Putting objects in context for open-vocabulary 3d detection. *arXiv preprint arXiv:2309.09456*, 2023a.
- Zhu, C., Wang, T., Zhang, W., Pang, J., and Liu, X. Llava-3d: A simple yet effective pathway to empowering llms with 3d-awareness, 2024a. URL <https://arxiv.org/abs/2409.18125>.
- Zhu, Z., Ma, X., Chen, Y., Deng, Z., Huang, S., and Li, Q. 3d-vista: Pre-trained transformer for 3d vision and text alignment. In *Proceedings of the IEEE/CVF International Conference on Computer Vision*, pp. 2911–2921, 2023b.
- Zhu, Z., Zhang, Z., Ma, X., Niu, X., Chen, Y., Jia, B., Deng, Z., Huang, S., and Li, Q. Unifying 3d vision-language understanding via promptable queries. *arXiv preprint arXiv:2405.11442*, 2024b.

Zou, X., Dou, Z.-Y., Yang, J., Gan, Z., Li, L., Li, C., Dai, X., Behl, H., Wang, J., Yuan, L., et al. Generalized decoding for pixel, image, and language. In *Proceedings of the IEEE/CVF Conference on Computer Vision and Pattern Recognition*, pp. 15116–15127, 2023.

## A. Appendix

|      |   |    |
|------|---|----|
| A.1  | Evaluation on 3D Instance Segmentation . . .                            | 15 |
| A.2  | Additional Implementation details . . . . .                             | 15 |
| A.3  | More details on Out-of-domain LX3D datasets                             | 15 |
| A.4  | Effect of Fine-tuning 2D backbones in Uni-<br>VLG . . . . .             | 16 |
| A.5  | Performance with different backbones . . . .                            | 17 |
| A.6  | Additional Metrics on ScanQA Dataset . . . .                            | 17 |
| A.7  | Visualizations of UniVLG on Referential<br>Grounding Datasets . . . . . | 17 |
| A.8  | Visualization of common failure modes of<br>UniVLG . . . . .            | 17 |
| A.9  | Performance analysis with pose and depth<br>noise . . . . .             | 17 |
| A.10 | Miscellaneous Details . . . . .   | 17 |
| A.11 | 2D-3D Generalization Test . . . . .                                     | 19 |
| A.12 | Discussion: Decoding Masks vs. Boxes . . .                              | 20 |
| A.13 | Evaluation with Mask based Intersection<br>Over Union . . . . .         | 22 |
| A.14 | Additional Related Work . . . . .                                       | 22 |

### A.1. Evaluation on 3D Instance Segmentation

We test UniVLG on 3D segmentation benchmarks of ScanNet200 (Rozenberszki et al., 2022) and Matterport3D (Chang et al., 2017) for instance segmentation tasks. These benchmarks have a fixed vocabulary of objects (200 classes in ScanNet200 and 160 classes in Matterport3D). SOTA models like ODIN (Jain et al., 2024) and Mask3D (Schult et al., 2023) train and evaluate in this fixed vocabulary setup by predicting a distribution over the fixed set of classes and supervising with softmax losses. PQ3D (Zhu et al., 2024b) evaluates in a language-prompted setup where they supply object names, one object at a time, and gather predictions for all objects in the vocabulary. They compare with a closed-vocabulary version of their model, and find that their language-prompted version is about 7% worse than their closed vocabulary version due to ambiguities in class names confusing CLIP (eg. “chair” and “armchair”; “table” and “desk” are different categories in ScanNet200). We follow PQ3D and evaluate our model in the language-prompted setup. The input to the model is a concatenation of all object classes of the benchmark as a long sentence (eg: “chair. table. sofa. bed. ....”). While PQ3D cannot predict multiple object classes simultaneously, and hence have to supply one object at a time, our model can simulatenously decode masks for all objects mentioned in the sentence. The results

are shown in Table-8 on the official validation splits of these benchmarks. We observe that UniVLG outperforms PQ3D in the language-prompted evaluation setup on ScanNet200.

### A.2. Additional Implementation details

UniVLG consists of 108M trainable parameters along with a frozen 220M parameter text-encoder (Koukounas et al., 2024) and a 304M parameter image-encoder (Oquab et al., 2024). For ablations in Table 7 and 5, we use a 88M parameter Swin (Liu et al., 2021) image-encoder. We train in data-parallel across 32 A100 80G GPUs with an effective batch size of 64. We use ScanEnts3D (Abdelreheem et al., 2023) version of ScanRefer (Chen et al., 2020a) and Referit3D (Achlioptas et al., 2020) which provides object annotations for all noun words in the language sentence. During training, we process either a sequence of  $N$  posed RGB-D images, or a single RGB image. During training, the model processes either a sequence of  $N$  posed RGB-D images or a single RGB image. For 2D images, we apply a 2D-to-3D lifting strategy with a 50% probability. When lifted, the images pass through all 2D-3D layers; otherwise, they remain in 2D space, skipping the 3D attention layers. At test time, we retain 2D images in their original space to prevent noise from predicted 3D pointmaps from impacting 2D performance. For 3D scenes, we compute CLIP embeddings for all images and captions and use this to select 5 relevant frames, with an additional 10 frames coming from Furthest-Point-Sampling (FPS) in the CLIP embedding space, for a total of 15 frames. At test time, we feed all images in a scene to our model. For validation results, we perform span prediction to identify the primary subject from a given utterance. We found that prompting an LLM (Dubey et al., 2024) with examples specific to a given dataset to result in better performance compared to traditional NLP libraries. We use Jina-CLIP (Koukounas et al., 2024) as the text-encoder, as it supports arbitrary input-length. We jointly train our model on all datasets, with text generation loss only active in question answering datasets. Our method provides for fast inference, with a *90-frame* scene taking  $\sim 1050$ ms and  $\sim 15$ GB of VRAM on an A100 GPU.

### A.3. More details on Out-of-domain LX3D datasets

Note: This collection of these out-of-domain datasets is not our contribution, but comes from a concurrent anonymous submission. We include the following details for the information of the reader.

The data is collected using an off-the-shelf annotation interface which allows for selecting rectangular regions on 2D videos and associating them with text. 3D instance masks are projected into 2D and shown alongside the RGB camera view. For ScanNet-GT (Dai et al., 2017), HM3D (Yadav et al., 2023) and ScanNet++ (Yeshwanth et al., 2023),

Table 8. Evaluation on 3D Instance Segmentation Benchmarks. (S) and (M) denotes models trained on sensor and mesh point clouds respectively.

| (a) ScanNet200    |                                       |             |             | (b) Matterport3D        |                                  |             |             |
|-------------------|---------------------------------------|-------------|-------------|-------------------------|----------------------------------|-------------|-------------|
|                   | Model                                 | mAP         | mAP25       | Input                   | Model                            | mAP         | mAP25       |
| Closed Vocabulary | Mask3D (Schult et al., 2023) (S)      | 15.5        | 24.3        | Closed                  | Mask3D (Schult et al., 2023) (S) | 2.5         | 10.9        |
|                   | Mask3D (Schult et al., 2023) (M)      | 27.4        | 42.3        |                         | Mask3D (Schult et al., 2023) (M) | 11.3        | 23.9        |
|                   | PQ3D (closed) (Zhu et al., 2024b) (M) | 27.0        | 46.3        | Vocabulary              | ODIN (Jain et al., 2024) (S)     | <b>14.5</b> | <b>36.8</b> |
|                   | QueryFormer (Lu et al., 2023) (M)     | 28.1        | 43.4        |                         |                                  |             |             |
|                   | MAFT (Lai et al., 2023) (M)           | 29.2        | 43.3        |                         |                                  |             |             |
|                   | ODIN (Jain et al., 2024) (S)          | <b>31.5</b> | <b>53.1</b> |                         |                                  |             |             |
| Language-Prompted | PQ3D (open) (Zhu et al., 2024b) (M)   | 20.2        | 32.5        | Language-Prompted       | UniVLG (Ours) (S)                | 10.7        | 24.5        |
|                   | UniVLG-3D-only (Ours) (S)             | 27.9        | 46.1        | UniVLG-2D-3D (Ours) (S) | <b>13.4</b>                      | <b>29.6</b> |             |
|                   | UniVLG (Ours) (S)                     | <b>31.0</b> | <b>52.1</b> |                         |                                  |             |             |

ground truth instance masks are used that are provided by the dataset. For ARKitScenes (Baruch et al., 2021), and ScanNet-SAM, instance masks produced by SAMPro3D (Xu et al., 2023) are used. Annotators have the ability to conglomerate multiple instance masks into a single object – this proved necessary for SAMPro3D segmentations, which tended to break large objects into many subparts. This is in line with ScanNet’s instance segmentation procedure in which annotators stitch together an automatically-generated oversegmentation of a 3D scene.

In addition to grounding the target object, annotators were asked to provide object grounding for all other nouns in the phrase they provided. For SAMPro3D masks, annotators could select any object they wished as a target. In later iterations of the task, for ScanNet and ScanNet++, a mask was highlighted in white with at least 1 distractor to serve as the target object for description. This is in line with prior literature which observed that the 3D referential grounding task is most challenging in the high-distractor case (Chen et al., 2020a).

While it was found that annotations on ScanNet and ScanNet++ were relatively reliable from a first pass, considerable mask/bounding box noise was observed when collecting annotations on SAMPro3D instance masks. To address this, a separate validation task was created. In this task, annotators saw a video similar to the video provided in the generation task, but only the selected masks for a particular language sample were highlighted. The referential expression description was also shown. This improved the quality of SAMPro3D samples substantially, but it also drastically slowed the collection rate.

### A.3.1. ANNOTATION SETUP

The annotation setup largely mirrors ScanRefer (Chen et al., 2020a) – annotators simply describe objects in a one-step fashion rather than the two-player game format of NR3D (Achlioptas et al., 2020). A 2D video interface was used for

the task, projecting 3D instance masks to 2D. Annotators can write full referring expressions and associate particular instance masks with particular tokens in the expressions. They may also agglomerate two or more instances into one.

When ground-truth instance masks are available (as in ScanNet and ScanNet++), these are used as the basis for annotation. When they are not available, instance masks are generated using SAMPro3D (Xu et al., 2023).

Decomposed by scene dataset, LX3D contains:

1. **ScanNet**: 4,470 language annotations covering 130 venues and 1038 objects for validation.
2. **ScanNet++**: 3,774 language annotations covering 50 venues and 1,303 objects for validation.
3. **ARKitScenes**: 1,416 language annotations covering 714 venues and 2,322 objects for validation.

### A.4. Effect of Fine-tuning 2D backbones in UniVLG

We study the effect of fine-tuning the 2D backbones on in-domain and out-of-domain performance. We train two versions of UniVLG with swin backbones, one with fine-tuning and the other without fine-tuning. For training, we use SR3D and NR3D, and evaluate on the validation sets of SR3D, NR3D (in-domain) and ScanRefer (out-of-domain). The results of the experiments are shown in Table-9. We find that both models work similarly well, both in-domain and out-of-domain.

Table 9. Effect of Fine-tuning 2D backbones of UniVLG for Acc@25 in Det Setup. SR3D and NR3D are in-domain and ScanRefer is out-of-domain

| Model               | SR3D | NR3D | ScanRefer |
|---------------------|------|------|-----------|
| UniVLG w/ finetune  | 65.6 | 52.7 | 54.4      |
| UniVLG w/o finetune | 66.7 | 52.0 | 54.5      |



### A.5. Performance with different backbones

We demonstrate that the performance can scale with the strength of the backbone. Specifically we use a DI-NOv2 (Oquab et al., 2024) backbone consisting of 1.1B parameters, scaling over 5x compared to the Swin backbone. To achieve high-performance during training, we freeze the backbone, although we note that it is possible that additional performance could be obtained with efficient fine-tuning techniques such as LoRA (Hu et al., 2021). In Table-10, we find that adding this backbone boosts performance on all 3 language grounding datasets, with substantial margins of 4.5%, 1.9%, and 3.4% @ 0.25 on SR3D, NR3D, and ScanRefer respectively.

### A.6. Additional Metrics on ScanQA Dataset

We report additional standard metrics used by ScanQA benchmark in Table-11.

### A.7. Visualizations of UniVLG on Referential Grounding Datasets

We show the visualization of UniVLG on 3D referential grounding in Figure-3 and on 2D referential grounding in Figure-4.

### A.8. Visualization of common failure modes of UniVLG

We identify three systematic failure modes in our model, illustrated in Figure-5.

- **Inclusion of distant outlier points in the predicted masks:** In the first image of Figure-5, while UniVLG accurately predicts the object, it also mistakenly includes some distant points in the mask. This leads to a larger bounding box during the mask-to-bounding box conversion in post-processing, negatively affecting accuracy metrics. Although our proposed box loss mitigates this issue, it doesn't fully resolve it.
- **Multiple instances of the same object being segmented together:** As shown in the middle image of Figure-5, UniVLG predicts both beds as a single output. Incorporating attention to language and queries helps reduce such errors, though they still persist. Our box loss also aids in addressing this issue.
- **Failures in language understanding** as seen in the third image of Figure-5.

The first two failure modes are specific to mask-decoding architectures, and similar issues have been noted by Mask3D (Schult et al., 2023) in their 3D instance segmentation tasks. Box-decoding architectures, on the other hand, generally avoid these problems. Nevertheless, we find that mask-decoding architectures offer significant advantages in other

aspects, such as more accurate and fine-grained segmentation, making them valuable despite these challenges.

### A.9. Performance analysis with pose and depth noise

To analyze the performance of UniVLG under sensor noise we conduct two experiments to model error in both pose and depth. For the pose error experiment, we add gaussian noise to the translation and rotation components of every camera pose in a scene. Similarly, for the depth error experiment, we add gaussian noise uniformly to the depth map. When each depth map is unprojected, the resulting point cloud becomes misaligned and performance decreases. We use relative pose error as defined in (Sturm et al., 2012).

We compare the robustness of UniVLG to prior state-of-the-art single-stage method of BUTD-DETR (Jain et al., 2022). We chose a single-stage method as our baseline, since multi-stage methods like PQ3D (Zhu et al., 2024b) and 3D-VisTA (Zhu et al., 2023b) rely on several external models, and use pre-processed intermediate outputs from them for their inference. This makes it harder to fairly run comparisons directly on the point cloud input. As shown in Figure-6, UniVLG is highly robust to both types of noise. At a mean error of 0.2, UniVLG impressively maintains a Top1@0.25 IoU accuracy of 66.7%.

In the pose error case, the model must understand the misaligned point cloud and cannot simply ignore the spurious points. However, UniVLG still shows impressive robustness with substantially less degradation compared to BUTD-DETR.

We believe a great portion of robustness comes from reliance on 2D pre-trained features and 2D layers in the network. Despite the noise in the depth and pose estimation, they still operate over the clean RGB images. Additionally, our 3D layers use local and relative attentions, which additionally contribute to the robustness.

### A.10. Miscellaneous Details

**Frame Sampling** To improve training efficiency, we opt to train on only a subset of available frames in each scene. This is critical, not only for reducing the average cost per step, but also in ensuring that the computations and memory is fixed per-step, allowing us to maximize the batch size and prevent waiting between GPUs in DDP. We initially tested a random selection strategy where each caption was paired with  $N = 15$  images from a given scene, with each scene originally containing around 90 frames. However, this change means that some sets of frames may no longer align with a given caption (i.e., the referenced object may not be visible in the selected frames). By simply ignoring instances where this mismatch occurs, this strategy performed remarkably well overall.

Table 10. Ablation of visual backbones on 3D language grounding. We evaluate top-1 accuracy on the official validation set without assuming ground-truth proposals (Det).

| Method          | SR3D         |              |              | NR3D         |              |              | ScanRefer    |              |              |
|-----------------|--------------|--------------|--------------|--------------|--------------|--------------|--------------|--------------|--------------|
|                 | Acc          | Acc          | Acc          | Acc          | Acc          | Acc          | Acc          | Acc          | Acc          |
|                 | @25<br>(Det) | @50<br>(Det) | @75<br>(Det) | @25<br>(Det) | @50<br>(Det) | @75<br>(Det) | @25<br>(Det) | @50<br>(Det) | @75<br>(Det) |
| UniVLG (Swin)   | 67.1         | 58.7         | 46.4         | 50.6         | 41.9         | 32.2         | 57.3         | 49.8         | 40.2         |
| UniVLG (DINOv2) | 71.6         | 63.8         | 49.4         | 52.5         | 43.3         | 34.2         | 60.7         | 53.2         | 42.6         |

Table 11. Extra Metrics on ScanQA validation set

|           | Method                       | EM          | BLEU-1      | ROUGE       | METEOR      | CIDEr       |
|-----------|------------------------------|-------------|-------------|-------------|-------------|-------------|
| Mesh PC   | 3D-LLM (Hong et al., 2023)   | 20.5        | <b>39.3</b> | 35.7        | 14.5        | 69.4        |
|           | PQ3D (Zhu et al., 2024b)     | 21.0        | -           | -           | -           | -           |
|           | 3D-VisTA (Zhu et al., 2023b) | 22.5        | 32.0        | 35.5        | 13.8        | 69.1        |
|           | NaviLLM (Zheng et al., 2024) | <b>23.0</b> | -           | <b>38.4</b> | <b>15.4</b> | <b>75.9</b> |
| Sensor PC | 3D-VisTA (Zhu et al., 2023b) | 21.6        | 30.1        | 34.1        | 13.2        | 65.3        |
|           | UniVLG (Ours)                | <b>25.7</b> | <b>36.1</b> | <b>40.0</b> | <b>15.2</b> | <b>78.5</b> |

However, to improve performance further, we sought to specifically include frames that were relevant to the caption (e.g., given "the red chair", we want to make sure all chairs in the scene are included), without biasing the model and causing a train/test distribution gap. To do this, we computed the CLIP embeddings of all scene frames, as well as the text embeddings of all captions. For a given caption, we select 5 relevant frames using the cosine similarity of these embeddings, ensuring that referenced entities are part of the selected frames. Moreover, to ensure diversity of frames and prevent the aforementioned bias, we select the remaining 10 frames using Furthest-Point-Sampling (FPS) on the CLIP image embedding space. We found fewer than 15 frames to slightly reduce performance, but that increasing beyond this point had no benefit.

**Language Encoder** As the original CLIP model only supported a maximum of 77 tokens, we opted to use Jina-CLIP which uses RoPE embeddings and is trained on 512 tokens.

**Matching Cost** Tuning the Hungarian matching cost weights turned out to be critical for 3D referential grounding. In prior works (Jain et al., 2024; Cheng et al., 2022), mask cost weights are typically higher than class cost weights. We find that it is important to have high class cost weights in referential grounding. This difference in costs is only required in Hungarian matching, we do not observe much benefits in changing the loss weights from what was used in the prior works.

**Mask Decoder design** Unlike prior works (Jain et al., 2024; Cheng et al., 2022), where object queries attend to visual features across multiple resolutions, we attend only to the highest-resolution feature scale. We explored multi-scale variants of our model but struggled to achieve good results, primarily due to difficulties in properly updating multi-scale visual feature maps with object queries and language tokens. Single-scale mask decoding approach is suboptimal for backbones like Swin, where attending to high-resolution feature maps is computationally expensive. However, with ViT backbones, where all feature maps share the same resolution, this limitation is less pronounced.

**Box Loss** As described in the main text, we employ the box loss to enhance the sharpness of the predicted masks. The box loss penalizes outlier points predicted by the mask head, which might not receive significant penalties through the mask loss alone. We incorporate the box loss into both Hungarian matching and the final loss used for backpropagation. Initially, we hypothesized that applying the box loss solely in Hungarian matching would suffice, as the bounding box is derived only from the extreme points of the predicted mask, resulting in sparse gradients during backpropagation. However, empirical results demonstrate that explicitly including the box loss in the final loss is beneficial. Notably, we use bounding box loss exclusively for 3D datasets and not for (lifted) 2D datasets. This distinction arises because lifted 3D point clouds can be noisy, potentially leading to inaccurate 3D bounding boxes.



Figure 3. Visualizations of UniVLG on 3D Referential Grounding Datasets of ScanRefer, SR3D, and NR3D The red masks indicate UniVLG’s prediction for the target object, and pink masks indicate its predictions for the anchor object. Green masks and boxes indicate ground-truth target and anchor objects.

Table 12. 2D-3D Generalization Test

| Model                       | 3D Sup. Classes | 2D Sup. Classes |
|-----------------------------|-----------------|-----------------|
| UniVLG                      | 72.6            | 53.8            |
| UniVLG w/o 2D-to-3D lifting | 71.4            | 0.0             |
| UniVLG (Upper-Bound)        | 69.7            | 84.2            |

### A.11. 2D-3D Generalization Test

We study the generalization between 2D and 3D domains using the 3D Instance Segmentation benchmark in the AI2-THOR simulator (Kolve et al., 2017). AI2-THOR consists of 120 object classes and provides posed RGB-D images of its 3D environments. We split these classes into two disjoint subsets: (a) 3D Supervised Classes (30) and (b) 2D Supervised Classes (90).

We train UniVLG in a 2D-3D setting where, for multi-view RGB-D inputs, the model is tasked with detecting objects

from the 3D Supervised Classes subset. For single RGB image inputs, it is tasked with detecting objects from the 2D Supervised Classes subset. At test time, the model is evaluated in a multi-view posed RGB-D setup on all 120 object classes to assess its generalization across the two subsets. Results are presented in Table 12.

We find that when UniVLG does not lift 2D images to 3D—simply skipping 3D attention layers in 2D batches, similar to ODIN (Jain et al., 2024) (row 2 in Table 12)—performance on 2D Supervised Classes drops to nearly zero. This suggests that without depth-based transformation, the model fails to learn from 2D supervision. However, when UniVLG incorporates depth information, its performance on 2D Supervised Classes becomes non-trivial, indicating that it successfully learns from 2D supervision and applies this knowledge in the 3D domain at test time.

In row 3, we report results for UniVLG trained in 3D on all



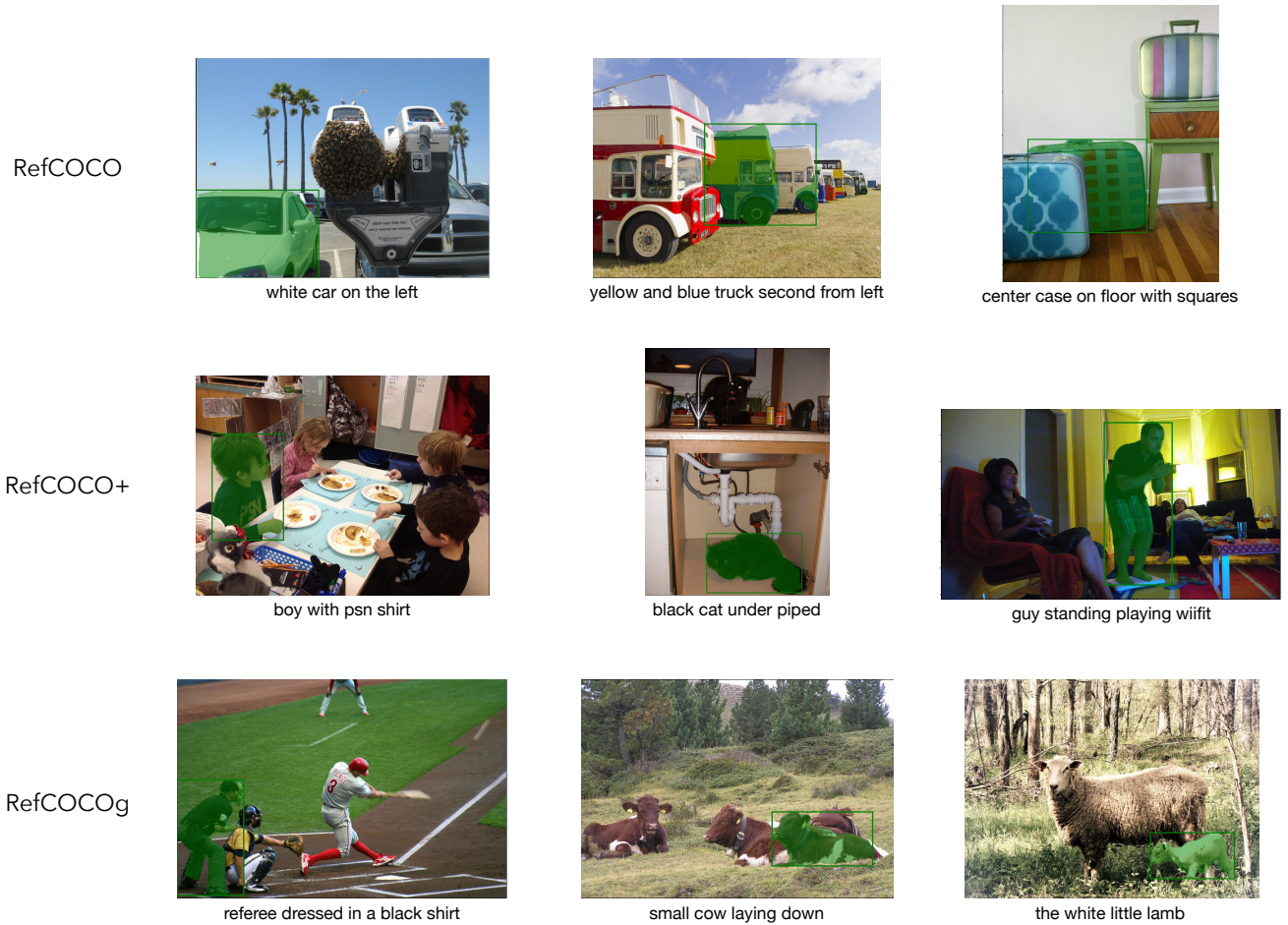


Figure 4. Visualizations of UniVLG on 2D Referential Grounding Datasets of RefCOCO, RefCOCO+, and RefCOCOg: The green masks indicate predictions of UniVLG.

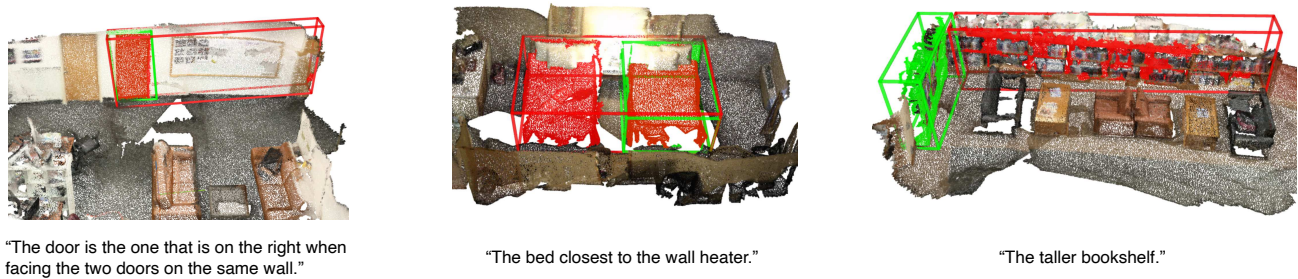


Figure 5. Systematic failure modes of UniVLG: Green boxes and masks are ground-truth, red masks and boxes are UniVLG’s predictions.

120 classes, representing an upper bound on its performance given full 3D supervision. We observe that UniVLG in row 1 remains significantly below this upper bound, highlighting the need for further improvements in 2D-to-3D generalization.

#### A.12. Discussion: Decoding Masks vs. Boxes

Decoding 3D bounding boxes has its advantages. For instance, datasets like Arkit3DScenes (Baruch et al., 2021) and Aria (Straub et al., 2024) only provide supervision for 3D boxes, making box decoding more favorable in such scenarios. However, recent methods such as Box2Mask (Chibane et al., 2022) demonstrate that segmen-



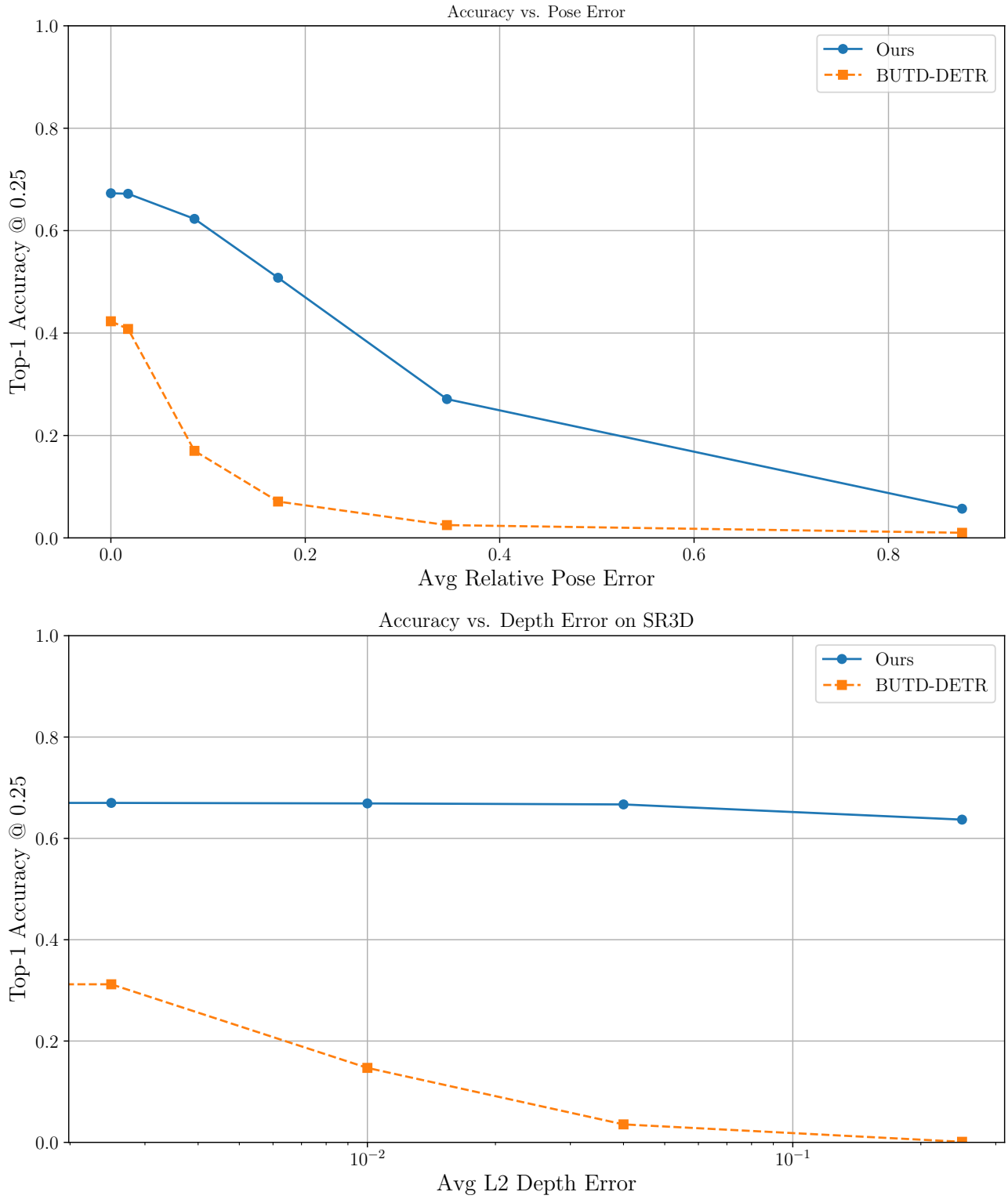


Figure 6. We analyze the performance of UniVLG and BUTD-DETR on SR3D as the pose and depth error increases. We add gaussian noise to the pose and raw depth which affects the unprojected point cloud that both models observe.

tation predictions can be effectively supervised using bounding box annotations alone, suggesting that the lack of mask labels may not pose a significant limitation. Despite this, we observe failure cases in mask predictions, such as outlier points being segmented in 3D or multiple instances of the same object being predicted as the answer (see Figure 5 in Appendix). These errors result in oversized or incorrect bounding boxes when masks are converted to boxes in a post-processing step, indicating the need for further research to address these issues in mask-decoding heads.

On the other hand, decoding masks offers significant benefits. As our experiments show, predicting masks leads to better performance compared to decoding boxes. Moreover, models like ODIN and UniVLG aim to unify 2D and 3D perception tasks, and mask prediction provides a consistent interface across these modalities. Masks represent per-point segmentation of pixels or points, whether in 2D or 3D, whereas box decoding requires separate prediction heads for 2D (4D outputs) and 3D (6D outputs), complicating unification efforts. Additionally, box-decoding heads are sensitive to normalization requirements for 3D scenes, such as mean-centering or scaling within a specific range (e.g., 0 to 1). Indoor and outdoor datasets, which vary significantly in 3D extents, often require separate decoder heads, further complicating training. In contrast, mask-decoding heads rely on cosine similarity between pixel/point features and object queries, making them more robust to variations in scene normalization and context. For example, UniVLG maintains strong performance even when input scenes are translated by 1000 meters, despite not being explicitly trained with translation augmentations. Furthermore, annotating 3D masks is easier for humans than annotating 3D boxes, especially with recent advances in interactive segmentation methods like SAM (Kirillov et al., 2023), which simplify the process of creating accurate mask annotations. This robustness, simplicity, and annotation efficiency make mask-decoding heads a preferable choice for unifying 2D-3D perception tasks.

### A.13. Evaluation with Mask based Intersection Over Union

While standard evaluations on existing 3D language grounding benchmarks rely on bounding box Intersection Over Union (IoU) for computing accuracy, we additionally report results using mask-based IoU for accuracy computation. The corresponding results are presented in Table 13.

### A.14. Additional Related Work

**Language Understanding Benchmarks** Vision Language Grounding is the task of localizing the objects mentioned in a language utterance in a given 2D or 3D scene. In the 2D domain, this task is primarily benchmarked on Ref-

COCO+/g datasets (Kazemzadeh et al., 2014) with humans annotating language instructions on top of COCO images. In the 3D community, this task is primarily studied in the popular benchmarks of SR3D (Achlioptas et al., 2020) containing programmatically generated sentences, and NR3D (Achlioptas et al., 2020) and ScanRefer (Chen et al., 2020a), containing human-annotated sentences, and 3D scenes from the ScanNet (Dai et al., 2017) dataset. The original benchmarks of SR3D and NR3D provide access to ground-truth bounding boxes of all objects in the scenes as input, and the task is to select the correct bounding box that corresponds to the language sentence. Most methods operate under this assumption, except for BUTD-DETR (Jain et al., 2022), which proposed directly predicting 3D bounding boxes instead of selecting from the available proposals. We follow BUTD-DETR and report results without assuming access to ground-truth boxes. The ScanRefer benchmark is similar to NR3D but does not provide ground-truth boxes as input. Recently, ScanQA (Azuma et al., 2022) and SQA3D (Ma et al., 2022) introduced 3D Question Answering Benchmarks. ScanQA focuses on spatial relations. SQA3D (Ma et al., 2022) provides pairs of situation descriptions and questions regarding embodied scene understanding, navigation, common sense and multi-hop reasoning.

**3D Question Answering and Captioning** For 3D question answering and captioning, approaches like PQ3D (Zhu et al., 2024b) and 3D-Vista (Zhu et al., 2023b) use small text generation heads on top of their language-contextualized features or queries to decode answers. Other approaches like 3D-LLM (Hong et al., 2023) and NaviLLM (Zheng et al., 2024) condense the visual scene features into a set of latent vectors and pass it to large pre-trained LLMs like BLIP2-flan5 (Li et al., 2023) or Vicuna-7B-v0 (Peng et al., 2023a). However, unlike 3D-Vista and PQ3D, they either get significantly poor performance on 3D referential grounding tasks (3D-LLM) or skip evaluating in that setup (NaviLLM). In this work, we follow PQ3D and 3DVista’s approach and use a small text generation head, mainly for its simplicity.

### Sensor vs Mesh Point Clouds in 3D benchmarks:

All the 3D benchmarks use point clouds derived from the 3D meshes provided by ScanNet (Dai et al., 2017). These meshes were constructed using several steps of post-processing over the raw sensor RGB-D data (which takes minutes-to-hours). In this work, we propose the first 3D language grounding model that operates directly over sensor RGB-D point clouds. For fair comparison, we benchmark other prior works with sensor point clouds as inputs, and show the benefits of using 2D pre-trained features for 3D language understanding tasks. These post-processing steps include mesh reconstruction and camera pose estimation, as well as several manual post-processing steps. These processes create fine-grained misalignments between the

Table 13. Mask mAP evaluation on 3D language grounding. We evaluate top-1 accuracy on the official validation set without assuming ground-truth proposals (Det).

| Method | SR3D         |              |              | NR3D         |              |              | ScanRefer    |              |              |
|--------|--------------|--------------|--------------|--------------|--------------|--------------|--------------|--------------|--------------|
|        | Acc          | Acc          | Acc          | Acc          | Acc          | Acc          | Acc          | Acc          | Acc          |
|        | @25<br>(Det) | @50<br>(Det) | @75<br>(Det) | @25<br>(Det) | @50<br>(Det) | @75<br>(Det) | @25<br>(Det) | @50<br>(Det) | @75<br>(Det) |
| UniVLG | 75.4         | 69.2         | 54.4         | 59.9         | 52.3         | 39.4         | 66.8         | 60.8         | 48.0         |

reconstructed mesh and the sensor RGB-D stream, resulting in drop in performance for methods operating over sensor RGB-D streams instead of the mesh point clouds, as also shown by prior works (Robert et al., 2022; Kundu et al., 2020b; Jain et al., 2024). This discourages the use of sensor RGB-D streams and thus the 2D features pre-trained on internet scale data. Using sensor point clouds directly is an emerging idea in the community, further bolstered by the recent introduction of datasets like EmbodiedScan (Wang et al., 2023) which also use sensor data directly instead of using meshes.